Review Article

Paul C. Uzoma#, Xiaolei Ding#, Baoshi Qiao, Emeka E. Oguzie, Yang Xu*, Xiaorui Zheng*, and Huan Hu*

AFM: An important enabling technology for 2D materials and devices

https://doi.org/10.1515/ntrev-2025-0154
received November 30, 2024; accepted March 4, 2025

Abstract: The last 20 years have seen remarkable progress in the study of 2D materials leading to the discovery of interesting properties and application potentials. However, there is still much to understand regarding these materials' physics, mechanics, and chemistry to utilize their full potential and make them useful to society. As a result, many efforts have been dedicated to using atomic force microscopy (AFM) to not only measure and study the properties of the 2D materials but also to assemble 2D materials heterostructures and optimize their properties for better performance. Therefore, this review discusses the various AFM methods that have been employed in this regard. It covers the following areas; the use of AFM to attach 2D materials on the AFM tip to study the interfacial friction and wear, AFM tip-based modification of the chemical and optoelectronic properties of 2D materials, and AFM manipulative scanning for 2D materials repositioning, interface cleaning, and smoothening. This review provides an up-to-date understanding of these new research areas and guides future research plans in 2D layered assembly.

Keywords: 2D materials, AFM, nanotribology, twistronics, optoelectronics

1 Introduction

The discovery of graphene in 2004 [1] has given the research community a platform to explore hundreds of other examples of 2D materials which include hexagonal boron nitride (hBN), phospherenes, xenes, and transition metal dichalcogenides (TMDC; *e.g.* WS_2, MoS_2, $MoSe_2$, *etc.*) [2–4]. The fascinating properties of these 2D materials have made them a reliable choice in the design of microelectrochemical systems and nanoelectromechanical systems (NEMS) for various purposes such as sensing, biomaterial, optoelectronic, tribology, *etc.* [5–7]. From an industrial viewpoint, remarkable progress has been made in the synthesis, device design, and applications of 2D materials [8]. However, a recent report from Naturephysics suggests that the past 20 years of 2D materials can be tagged "disappointing" in terms of making a huge impact on commercial products [9]. For instance, the European Research Consortia's Graphene Flagship with the mandate to "bring graphene innovation out of the lab and into commercial applications" has not met its 2020s target of impactful commercialization [9]. One major limiting factor is that much more fundamental physics of 2D materials is yet to be understood [9,10]. This is because, the atomically thin 2D materials layers are atomically close, so, the physical, mechanical, and chemical interactions develop simultaneously and influence each other, resulting in a broad range of topological structures and properties across nanoscale and microscales [11]. Therefore, it is crucial to understand the physics, mechanics, and chemistry of these "wonder materials" to utilize their full potential and make them useful to society.

# These authors contributed equally to this work and should be considered first co-authors.

*** Corresponding author: Yang Xu,** ZJU-UIUC Institute, International Campus, Zhejiang University, Haining, 314400, China; College of Integrated Circuits, Hangzhou Global Scientific and Technological Innovation Centre, Zhejiang University, 38 Zheda Road, Hangzhou, 310027 China, e-mail: yangxu-isee@zju.edu.cn
*** Corresponding author: Xiaorui Zheng,** Key Laboratory of 3D Micro/Nano Fabrication and Characterization of Zhejiang Province, School of Engineering, Westlake University, Hangzhou, Zhejiang, 310024, China, e-mail: zhengxiaorui@westlake.edu.cn
*** Corresponding author: Huan Hu,** ZJU-UIUC Institute, International Campus, Zhejiang University, Haining, 314400, China; State Key Laboratory of Fluidic Power & Mechatronic Systems, Zhejiang University, Hangzhou, China, e-mail: huanhu@intl.zju.edu.cn
Paul C. Uzoma: ZJU-UIUC Institute, International Campus, Zhejiang University, Haining, 314400, China; Africa Center of Excellence in Future Energies and Electrochemical Systems (ACE-FUELS), Federal University of Technology, PMB 1526, Owerri, Imo State, Nigeria
Xiaolei Ding, Baoshi Qiao: ZJU-UIUC Institute, International Campus, Zhejiang University, Haining, 314400, China
Emeka E. Oguzie: Africa Center of Excellence in Future Energies and Electrochemical Systems (ACE-FUELS), Federal University of Technology, PMB 1526, Owerri, Imo State, Nigeria

One important approach for studying 2D materials is atomic force microscopy (AFM). Based on the earlier design of scanning tunneling microscopy, in 1985, Binning, Gerber, and Quate invented AFM which measures the forces between an AFM tip and a sample's surface [12]. AFM has become a prominent surface profiler for topography and normal force measurements on the micro to nanoscale ever since [13,14]. Over the years, the AFM has been modified to study lateral(friction) and adhesion forces [15,16], analyze surface scratch and wear [15], and measure elastic and plastic properties such as indentation, hardness, and modulus [13,17–20]. AFM can also offer direct structural information on the molecular functionalization of 2D materials [21]. For instance, the tribology of contact interfaces has been studied for centuries, however, the arrival of AFM enabled the assessment of the principal atomic activities that control interface friction and wear thereby validating the many existing friction theories [22]. AFM is very efficient in tribology because the atomic-sized ultra-smooth AFM probe makes single asperity contact with the counter surface in contrast to most interfaces where multiple asperity contact is made [23]. This single asperity contact offered the required platform to analyze the commensurability of the sliding surfaces and how it affects friction [24], investigate the jump-to-contact phenomenon on soft materials [25], study detachment force in thin films [26], examine the tribochemical reactions at the interface [27,28], study the effects of sliding velocity [29], and measure the true contact area and the interfacial shear strength [30,31]. For example, Rejhon *et al.* [32] employed AFM to measure the relationship between the interfacial shear modulus and friction force in 2D layered materials which is otherwise difficult to measure. They proved that the interfacial shear modulus is significantly influenced by the chemistry, stacking order, and the interaction between the atomic layer and the substrate. This study of the atomic level interactions is vital in the design of NEMS.

Furthermore, AFM has been employed to exploit and maneuver individual atoms of molecules and materials in order to improve target properties [33–36]. Readers are encouraged to read recent reviews from Li *et al.* [37] for an explanation of the working mechanisms of the AFM nanofabrication of 2D materials, Wu e*t al.* [38], and Wu *et al.* [39] for discussion on the different mechanical properties that can be obtained when AFM is used to characterized 2D materials. However, this work focuses on the ingenuity of researchers in manipulating AFM techniques to study, modify, and optimize the surface properties of 2D materials in order to achieve their research objective as described in Figure 1. Sections 2 and 3 discussed the use of AFM manipulating scan to (i) attach 2D materials on the AFM tips to study friction and wear at the interface of 2D materials, (ii) control the lattice orientation of 2D materials to study the twist angle-dependent properties and (iii) reposition the 2D materials on a substrate. The following three Sections (4–6) explored several cases where AFM tips were used to (i) modify the surface chemistry of 2D materials, (ii) induce strain in 2D materials to optimize the optoelectronic behavior and (ii) clean and smoothen the interfaces of 2D materials to enhance the electronic properties of devices. Finally, Section 7 discussed the various challenges currently limiting AFM applications in 2D materials and offered valuable suggestions to guide future research plans in 2D layered assembly.

2 Tip's surface reconstruction for interface tribology

Graphene/MoS_2, graphene/h-BN, and WS_2/graphene heterostructures with varying lattice dimensions are known to provide an incommensurate contact, offering a path to achieve extremely low friction, also known as superlubricity. Normally, the contact condition of 2D materials/2D materials is required to determine the friction at the interface of 2D materials layers. So, researchers have developed ways of coating AFM tips with 2D materials to measure the interlayer properties. Nonetheless, it is very challenging to obtain a well-defined defect-free single crystalline contact interface between 2D material layers to visualize and assess the intrinsic interlayer friction and material transfer activities. For instance, Hui *et al.* proposed dipping AFM probes into high-quality solution-processed graphene [46]. Although this method ensures the attachment of graphene flakes at the tip apex, it leaves excesses of graphene on the cantilever (Figure 2(a)), likely affecting the AFM laser reflection. Wen *et al.* [47] grew a graphene layer on Au-coated AFM tips using the chemical vapor deposition method. Growing CVD graphene on copper and transferring it onto an AFM tip has also been explored [48]. Yu *et al.* [49] proposed using a micromanipulator set-up to pick up graphite flakes onto a microsphere probe (Figure 2(b)). Liu *et al.* [50] prepared graphene-coated microspheres as described in Figure 2(c) and used the AFM lateral scan to examine the friction properties. The resultant microsphere is big (8 μm diameter), rough, and can achieve multiple asperity contact with the counter surface, giving rise to superlubricious incommensurate interfaces. One crucial limitation of the above-mentioned techniques is the low

quality of graphene. The CVD carbon film grown directly on the tip has a lower quality than the one grown on copper [46,51]. Also, the transfer of graphene on the tip will most likely leave some unwanted contaminants on the graphene [52]. Therefore, some studies have shown different ways of overcoming these challenges using the AFM technique.

Tian *et al.* [53] showed that superlubricity of 2D materials can be achieved by adhering graphene on an AFM tip to form interlayer friction heterojunction. They used a Silicon AFM tip to scan HOPG with an ultra-low friction coefficient as described in Figure 2(d). Their goal was to employ the shear effect to trigger strong peeling energy on the surface of the HOPG thereby forming a reconstructed tip bearing attached graphene layers as shown in the High-resolution transmission electron microscopy (HRTEM) image (Figure 2(d)). In this case, under the pre-sliding actions of the Si tip against the HOPG, there was forced exfoliation of graphene layers from HOPG which bonded to the AFM tips. This was followed by a fast accumulation of the transferred films around the tip during the initial friction stage. The friction between the newly reconstructed tip (graphene-transferred tip) and the heterojunction designs ($Gr/Ws_2/Si$, $WS_2/Gr/Si$) proved superlubricious with 0.003 coefficients of friction. However, the adhesion of the transferred graphene to the tip is very weak.

Employing a heating process, Liu *et al.* [54] overcame the problem of weak adhesion encountered by Tian and colleagues. They used the thermally assisted mechanical exfoliation and transfer approach described in Figure 2(e) to wrap various 2D flakes around AFM tips to study the interlayer friction. The heating process ensured the flakes adhered strongly to the tips. Their findings confirmed superlubricious behavior between the 2D materials films and bulk materials. Also, angular dependence superlubricity was observed between graphite layers whereas

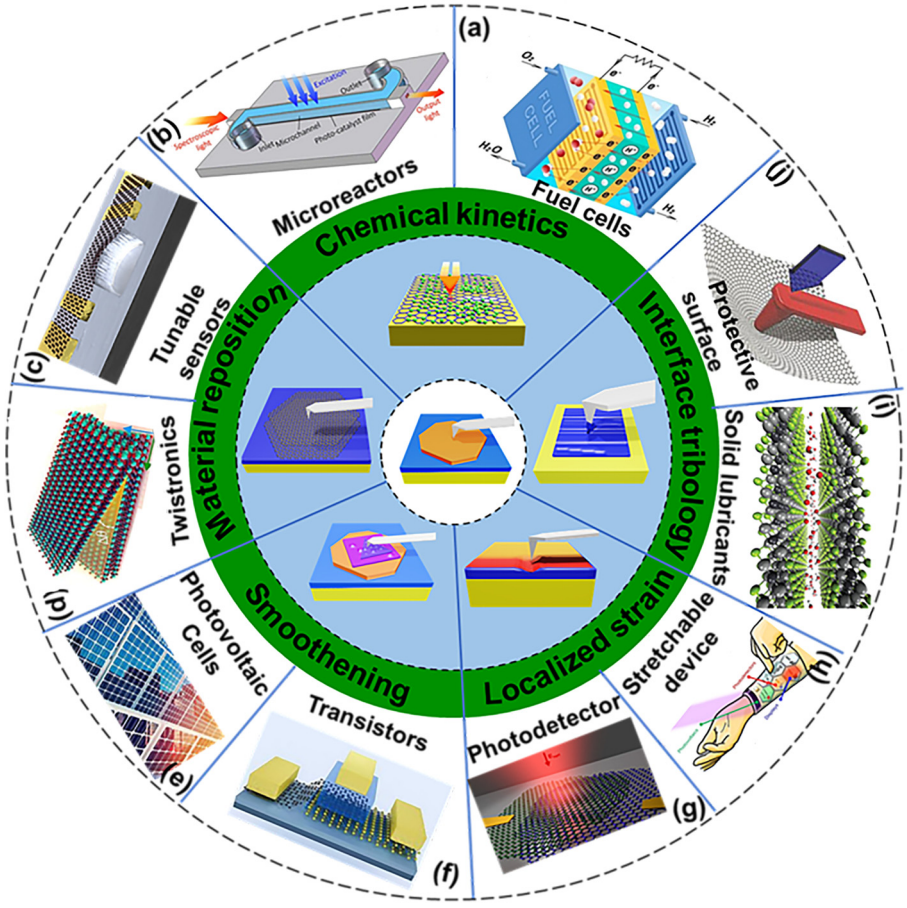

Figure 1: Various AFM tip-based treatments and applications. Image illustrations of (a) polymer electrolyte membrane fuel cells (Image credit @MathWorks), (b) microreactor [40], (c) graphene-based pressure sensor (Image credit S. Wagner@AMOGmbH), (d) twisting of 2D materials layers [41], (e) photovoltaic cells, (f) transistor designed with graphene (black hexagons) and MoS_2 (blue and yellow structures)(Image credit@University of Buffalo), (g) van der Waals heterojunction photodetector [42], (h) wearable stretchable device [43], (i) Mxene as solid lubricants [44], and (j) protective ability of 2D materials [45].

angular independent superlubricity was seen between graphite flake and bulk h-BN substrate. This was attributed to the incommensurate contact of the distinct lattices. The inherent incommensurability between h-BN and graphite described the independence of the superlubricity on the relative rotation angle [55]. Furthermore, the superlubricity between the graphite flakes was found to be stable over a prolonged period without torque-associated reorientation which is a result of good adhesion with the Si tip occasioned by heating.

Sheehan and co-workers developed an AFM technique for assessing the interfacial friction of molybdenum trioxide (MoO_3) nanometer crystals deposited on molybdenum disulfide (MoS_2) and Molybdenum diselenide ($MoSe_2$) [22]. It is worth noting that MoO_3 whose a-axes are ~15° with reference to the a-axes of underneath MoS_2 is mostly known to undergo lattice-directed sliding (LDS). In LDS, the movement of one 2D material's nanocrystal is confined along one of the crystallographic axes of the underlying 2D material. This confinement is a result of a higher level of commensurability that exists between the two-layered materials along only one axis of the interface. This organized movement provides a better platform to study chemical and physical interface coupling while avoiding issues of crystallinity and interface alignment. They investigated the force needed to shift MoO_3 nanocrystals during LDS and gave an understanding of certain atomic-level processes affecting friction. Their strategy was to weakly append the MoO_3 nanocrystal onto the AFM tip as described in Figure 2(f) and, thereafter, easily move the nanocrystal along one axis of the MoS_2 or $MoSe_2$ substrates while it is firmly held perpendicular to this axis.

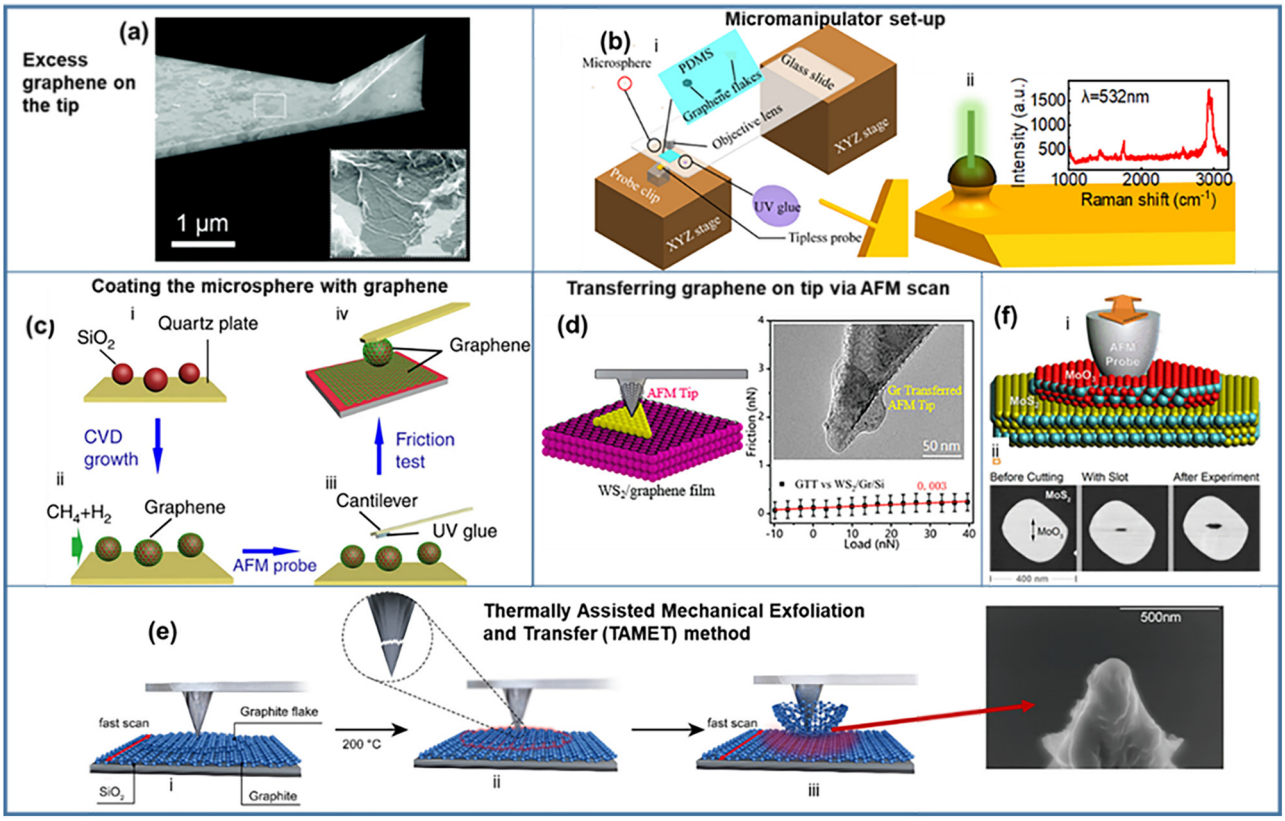

Figure 2: (a) SEM image of an AFM tip with the cantilever coated with excess graphene [46]. (b) Schematic illustration of a micromanipulator used for the fabrication of graphite-coated microsphere probe [49]. (c) Design schematics and friction test of the graphene-coated microspheres; First step: Dispersion of SiO_2 microspheres on quartz plate, Second step: Growth of multilayer graphene film on the microspheres using the CVD method, Third Step: Using UV light solidify glue to attach the AFM cantilever to the microspheres, and Fourth Step: Friction measurement [50]. (d) Schematic representation of the use of bare Si AFM tip to scan highly ordered pyrolytic graphite (HOPG), the HRTEM of the tribolayer-wrapped tip and the friction/load plot [53]. (e) Schematic representation of (i) scanning of tip on the graphite substrate; (ii) fracture of the tip during the rapid heating process; (iii) The flakes wrap around the tip as it scans under high temperature and the SEM image of graphene-wrapped tip [54]. (f) (i) The experimental representation of the AFM tip cutting a slim cut in the MoO_3 nanocrystal which was later moved along the easy path of the underneath 2D material lattice; (ii) The AFM images showing the molybdenum trioxide (MoO_3) nanocrystals prior to cutting, after cutting the slim slot, and after the friction test [22].

Their findings showed an expected linear increase in the lateral force needed to move the nanocrystal with respect to the area of the nanocrystal. Also, the interfacial shear strength was observed to be much lower than what is obtained in a macroscale system and it is strongly dependent on the velocity and duration of sliding [56,57].

3 Tip-based manipulative scanning for lattice orientation control and materials repositioning

The study of the influence of twist angles on the electronic properties of 2D materials commonly referred to as "Twistronics" has attracted huge research interest in recent years [58,59]. The lattice mismatch and rotation between layers of 2D materials can lead to high wavelength moiré superlattices which can significantly change the electronic response of the vdWHs, leading to device characteristics that are radically different from those of the constituent layers [60,61]. Such unique properties include superconductivity [62,63], moiré exciton [64–66], magnetism [67,68], and fractional Chern insulating states [69]. For instance, the significance of rotational alignment between insulating and conducting 2D layers has been demonstrated using graphene and hBN. vdWHs formed using graphene on hBN show a rotation-dependent moiré pattern (Figure 3(a)) [70]. Their closely comparable lattice constants are confirmed to form a large moiré superlattice that evolves near zero angle mismatch [71], extensively altering the band structure of graphene, creating an energy gap at the charge neutrality point (CNP), and forming replica Dirac points at higher energies [72–74]. The "tear and stack" approach is mostly used in constructing twist devices [75,76]. However, the twist angle obtained using this method is no longer tunable after the fabrication of the device. Hence, one has to construct multiple devices with different twist angles to examine twist-angle-dependent properties. This can result in other external factors instead of pure twist-angle effects influencing the outcomes. Interestingly, the AFM manipulation technique has been shown to provide *in situ* layer orientation control in vdWHs assembly and experiments [77,78]. For example, Du *et al.* [79] used an AFM manipulation approach to rotate the as-grown non-twisted MoS_2 on few-layer graphene to show the interlayer twisting angle dependence of photoluminescence (PL) and Raman spectra as seen in Figure 3(b). The intensity of the PL and the emission energy were found to increase with increasing twisting angle, while there is a decrease in the splitting of the E_{2g} mode. These observations are due to the twisting angle-dependent interlayer forces and misorientation-associated lattice strain between the graphene and MoS_2. Yuan *et al.* [80] also confirmed the dependence of PL and Raman spectra on the MoS_2/graphene interlayer twisting angle. They further took advantage of the superlubricity property of the MoS_2/graphene interface to precisely control the twist angle with very high accuracy in the order of 0.1°.

In a bid to provide easy control of the lattice orientation, Rebeca and co-workers used a preshaped BN layer to fabricate BN/graphene/BN vdWHs [81]. The preshaped topmost BN layer has arms to enable easy AFM manipulation as shown in Figure 3(c), hence pushing one arm rotates this layer and alters its crystallographic alignment with respect to the underneath layer of graphene. Their fabricated tunable device exhibited on-demand control over the length of the moiré potential hence offering dynamic tunability of the electronic, optical, and mechanical properties of the system. Similar designs with a rotatable device have also been reported for different vdWHs assemblies: monolayer graphene sandwiched between two crystals of BN where the top BN has rotatable arms [86] and graphene monolayers divided by hBN gear with center-opening as described in Figure 3(d) [82]. Recently, Kapfer *et al.* [83] demonstrated the manipulation of the moiré patterns in hetero- and homobilayers through in-plane bending of monolayer ribbons, using an AFM tip (Figure 3(e)). Their method ensures continuous variation of twist angles with enhanced twist-angle homogeneity and decreased random strain, leading to moiré patterns with tunable wavelength and very low disorder.

Furthermore, Cherepanov *et al.* [84] showed the use of an AFM manipulative scan to disassemble 2D nanoparticles that aggregated into multi-nanometer particles during synthesis (Figure 3(f)). Their experimental results proved that AFM is effective for splitting self-assembled nanoaggregates and moving the target nanoparticles to destinations on the substrate which will greatly aid in the design of solid lubricants. Regarding the dissembling of 2D materials heterostructures, Li *et al.* [87] proved that the vdW interaction is stronger between graphite and MoS_2 than between graphite and hBN irrespective of their relative stacking orientations. They employed a graphite-wrapped AFM tip to confirm that the critical adhesion pressure between 2D heterostructures is in this order: MoS_2/graphite > BN/graphite > graphite/graphite. Their finding is in agreement with the Liftshiz theory-based predictions which suggest that the dielectric functions of the materials play a significant role in the interactions of the vdW at heterointerfaces [88,89].

Kawai *et al.* [90] employed an AFM lateral manipulative scan to show the superlubricity of GNR during sliding contact on a gold substrate. They fastened the AFM tip to the ends of the target GNRs and performed a controlled back-and-forth dragging while recording the friction force. Their results proved superlubricious behavior between the GNR and gold with both values of static and kinetic friction force within the 100-pN range. Also, they observed that the dynamics of the sliding motion are affected by the extent of commensurability arising from the surface reconstruction. Inspired by the work of Kawai and co-workers, Gigli *et al.* [85] used classical MD simulation to perform frictional manipulation of the GNR on gold substrate set-up as shown in Figure 3(g). This is to give the theoretical clarification on the evolution of stick-slip emanating from the short 1D edges instead of 2D bulk, the influence of adhesion, lifting, and bending elasticity of graphene on the GNR sliding friction. At small lifting height, they explained that the symmetric back-and-forth frictional response arises from the limited degree of elastic deformations aggregated by the GNR when dragged against an energy barrier. However, when the lifting height is increased, there is a decrease in

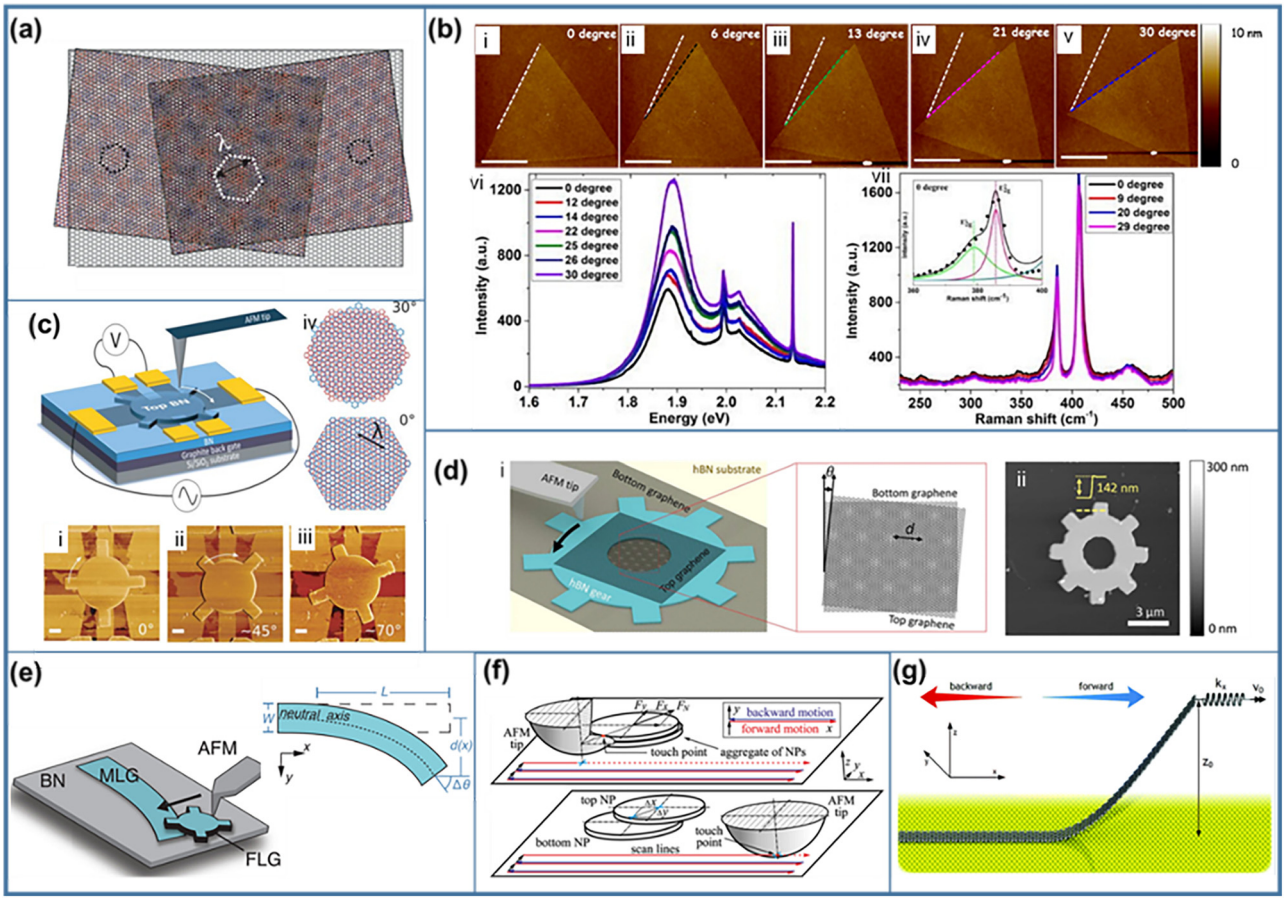

Figure 3: (a) Schematic illustration of doubly aligned bilayer graphene with hBN placed at the top and bottom. The black and the white hexagons show the primary moiré and supermoiré plaquettes, respectively [76]. (b)i–v. Twisting angles achieved *via* AFM tip manipulation. Plots showing: vi. the dependence of PL on the interlayer twisting angle, vii. Raman spectra dependence on the interlayer twisting angle. The inset is Lorentzian fitting of the splitting E_2g, and the splitting of E_2g against interlayer twisting angles [79]. (c) Cartoon image of the rotatable heterostructure and the experimental procedure, i–iii. AFM image of the device depicting three different orientations of the topmost hBN, iv. Schematic images of the moiré superlattice emanating between the graphene (red) and hBN (blue) at zero angle. λ is the moire wavelength [81]. (d) Schematic representation of a tunable bilayer graphene device consisting of two graphene monolayers separated by hBN gear on another hBN substrate. There is the formation of moiré superlattice of period "d" at the overlapping area in the center of the gear. ii. The topographical image of the twistable device [82]. (e) Schematic image showing bending of a 2D material ribbon using a nanomanipulator and AFM tip [83]. (f) Schematics of the relative position of the nanoparticle aggregate and the AFM tip during its scan line movement; top – at the start of the push and bottom- completion of the push [84]. (g) Schematic representation of the molecular dynamics (MD) simulation setup: the AFM tip lifting the graphene nanoribbon (GNR) at one end and laterally pulling it. The lifted end of the GNR is attached to one side of a soft spring, and the other side of the spring moves at a constant velocity thereby dragging the GNR back and forth [85].

the bending energy needed to deform the GNR resulting in different driving mechanical responses for the two opposite scan directions. On achieving the required minimum energy to initiate sliding also known as the Peierls–Nabarro barrier [91], the sliding dynamics generated asymmetric features in the emanating stick-slip regime for the forward and backward dragging. Expanded period of the stick-slip regime and the likely manifestation of the "peeling" effect in the backward trace for raising the lifting height are the major consequences of this improved elastic deformation.

4 Tip-induced surface chemistry modification

Mechanochemistry is a process of driving chemical reactions using mechanical force in place of heat, light, or electric field. In recent years, AFM has been employed in mechanochemistry to drive and assess *in situ* chemical processes thereby shedding light on local electrochemical kinetics and local electron densities [92–96]. Notably, achieving a broad insight into how to drive and assess reactions at the nanoscale level under different conditions will significantly aid in the designs of highly efficient chemical reactors [97], flexible electronics [98], batteries and supercapacitors [99,100], fuel cells [101], biomaterials [102], and lubricants [103]. For example, in semiconductors and conducting materials, researchers have shown that it is feasible to locally initiate the adsorption of hydrogen or oxygen groups using a conductive AFM tip in contact with a surface confirming it to be a fitting platform to investigate the link between the applied local strain and electrochemical reactivity [104,105]. AFM approach is ideal for studying these chemical processes because it can precisely control the applied stresses and reaction durations, and can conveniently assess the reactions happening on monolayers, surfaces, or other nanoscale systems without the need to grind into smaller structures [106].

Tang *et al.* [107] recently used a chemically active SiO_2 microsphere to initiate chemical reactions on a graphene monolayer to show that the wear susceptibility at the atomic step edges is significantly influenced by the mechanochemistry of frictional interfaces (Figure 4(a–c)). Due to the mechanochemistry effect, the critical contact stress needed to cause wear at the graphene step edges was confirmed to be largely decreased from ~8.8 GPa for mechanical wear to ~0.28 GPa, suggesting a decrease in the graphene's resistance to wear. Felts *et al.* [27] demonstrated the use of the AFM technique to cleave different functional groups on chemically modified graphene (CMG) sheets and to show how the character of the arbitrary organic bonds affects its scission (Figure 4(d–g)). Regarding friction on CMGs, researchers have confirmed that the added chemical groups relate more firmly with the tip than graphene, thereby increasing the friction [108–110]. Since pristine graphene possesses a lower friction value than the CMGs, observing the friction offered direct *in situ* measurements of the local chemistry. Prolonged scans and higher loads were found to lead to more functional group removal. The difference in friction between CMG and pristine graphene was shown as a direct estimate of the extent of functionalization, where lower friction values coincide with fewer chemical groups on the graphene surface. They proved that greater forces are needed for higher bond energies, and lower forces are required for longer bond lengths as previously confirmed by Beyer and Clausen-Schaumann [111]. Besides, the obtained trend in the contact stress was found to correspond to the data obtained from the density functional theory (DFT) calculations of bond length and bond energy studied by other researchers [112,113]. In continuously altering the mechanochemical reaction rate by tuning the normal force and dwell time during AFM contact-mode scan on CMG, Kim *et al.* proved the possibility of a gradient mechanochemical cleavage in large-area CMG sheets [114].

Raghuraman *et al.* [116] used sliding of conductive AFM on multilayer graphene sheets to examine the influence of applied stress on the kinetics of the surface oxygen evolution reaction. The experiments showed the accumulation of oxygen groups on the surface, and the oxygenation rate increased with the applied force. Also, the rate was found to be higher at the local edges and defects than at the basal plane indicating non-uniformity of the oxygenation rate. The group had earlier reported on the use of the AFM technique to determine reaction kinetics at nanoscale [115]. Their initial results showed shifts in relative friction for heater temperatures 300 to 375°C with respect to tip dwell time (Figure 4(h–p)). Also, the reaction rate with respect to the heater temperature showed a strong exponential dependence (Figure 4(m)). Furthermore, they designed a nonisothermal, nanoscale thermal desorption microscopy (ThDM) technique to overcome the drawbacks of the thermal approach [115]. The ThDM technique was believed to speedily determine the temperature dependence of reaction rate during a tip temperature or force ramp by employing the fundamentals from bulk thermal analysis methods such as temperature-programmed desorption [117] and thermogravimetry [118,119]. Herein, increasing the tip's temperature or force linearly between each scan offered an estimate of the reaction rate with respect to either tip's temperature, force, or both as shown in Figure 4(n–p). Their results proved that the sliding tip

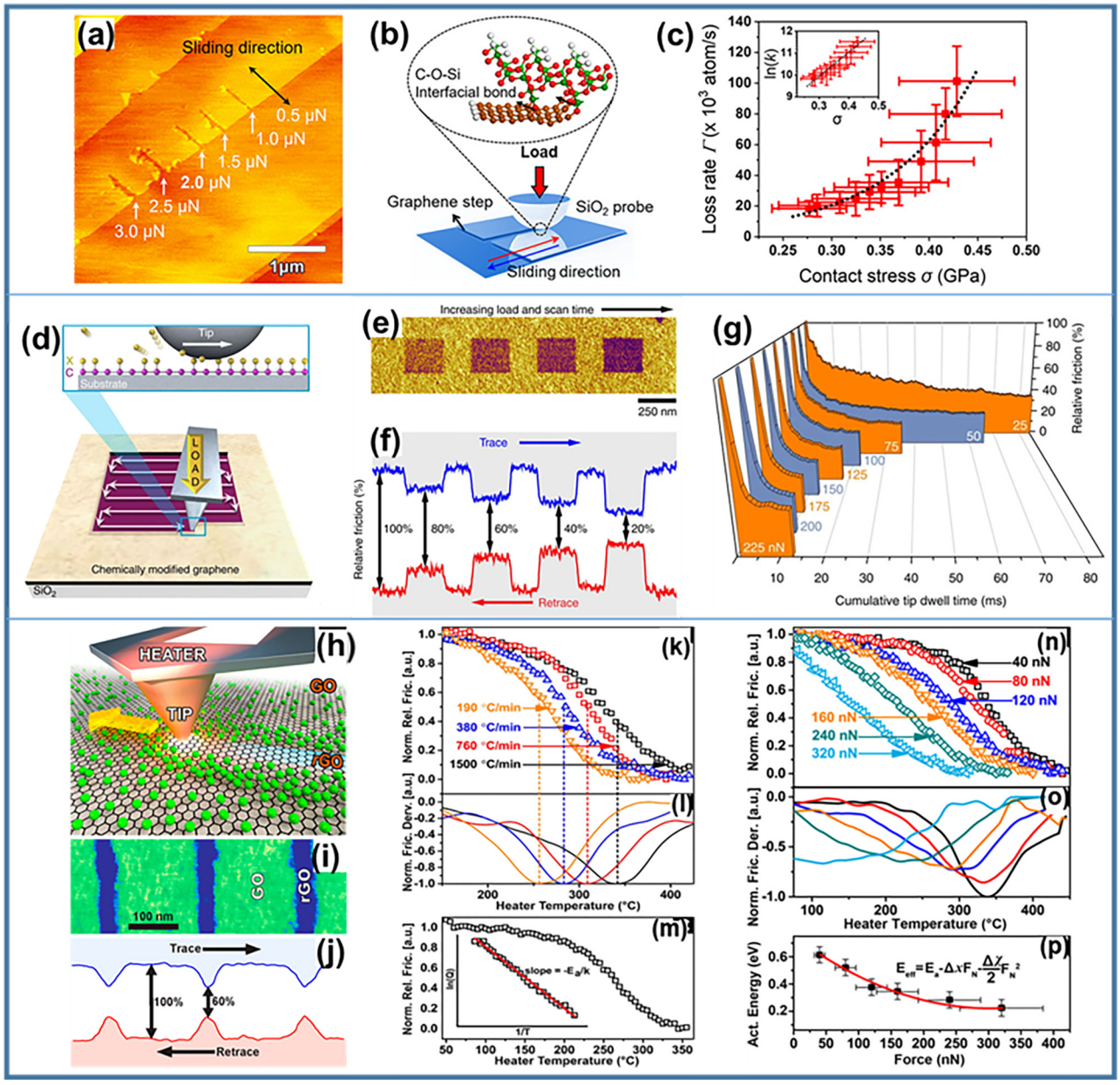

Figure 4: (a) AFM images of the nanochannels fabricated at 0.5–3.0 μN normal loads. (b) Schematic of the mechanochemically stimulated atomic attrition mechanism at the SiO_2 probe and monolayer graphene interface. (c) Plot showing that the rate of reaction (k) of monolayer graphene is dependent on the exponential contact stress. The inset shows a linear relation between the ln(k) and contact stress [107]. (d) Illustration of the mechanochemical activities where a tip with a known normal force takes away the functional groups from a CMG film. (e) Lateral scan on oxygenated graphene with areas decreased with increasing contact stress and scan period. (f) A line scan of the four squares shows a ~5x decrease in friction because of oxygen group removal. (g) A plot of relative friction with respect to tip dwell time for normal loads reveals an exponential increase in decay rate with increasing normal load [27]. (h) Schematic drawing showing the reduction by a heated AFM tip, where pressure and heat locally remove the oxygen groups. (i) Image of friction force image showing the patterns of the reduced GO. (j) 60% friction drop attributed to oxygen group removal. (k) Normalized plot of the relative friction with respect to the heater temperature for different ramp rates. (l) Normalized plot of the relative friction derivative revealing a rightward move in maximum removal with increase in ramp rates. (m) Constant heating rate plot, The inset shows the calculation of activation energy using the estimated interface temperatures. (n) 760°C/min constant heating rate plots for various tip forces. (o) Normalized derivative of the relative friction revealing a change in maximum removal toward lower temperatures for increasing tip force (p) Plot of the obtained activation energy with respect to tip force revealing a nonlinear reduction in activation energy with increasing force [115].

detached oxygen groups through a first-order process with an activation energy of ~0.6 eV which significantly deviates from bulk analysis, where oxygen reduction is a second-order process with >1.3 eV activation energy [120,121]. This suggests that the sliding tip drives oxygen reduction through a different pathway. Higher loads were shown to impede the reaction pathway nonlinearly suggesting that it is inappropriate to infer a linear correlation between applied load and energy barrier for surface oxygen reduction. This observation is generally known as the Hammond effect, herein, the increase in the applied force changes the energy levels of both the reaction and transition states, thereby changing the minimum reaction trajectory and decreasing the force dependence of the activation barrier [122,123].

It is worth expressing the different mathematical models that appropriately describe the mechanochemical reactivity that guides the design of the experiments used in driving and assessing the mechanochemical reaction rates. Equation (1) describes the drop in the relative friction as a function of time at a given temperature.

$$\Delta f(t) = Ae^{-\lambda t} + y_0. \tag{1}$$

In which Δf, λ, and t represent the relative friction, reaction rate, and cumulative tip dwell time, respectively. The cumulative tip dwell time (t) is the total time spent by the tip at a given point and is expressed as:

$$t = 4N_s\frac{\pi a^2}{vp}. \tag{2}$$

In which N_s, a, v, and p are the number of AFM scan images, the radius of the tip, the velocity of the tip, and the pitch between scan lines respectively. So using equation (1) to fit the plot of relative friction against the cumulative tip dwell time gives the reaction rate as slope as demonstrated by Raghuraman *et al.* [115] and Felts *et al.* [27].

Equation (3) is the Arrhenius thermal activation model used in obtaining the activation energy [103,121].

$$\lambda = \lambda_0 \exp\left(\frac{E_a}{kT}\right). \tag{3}$$

In which E_a, k, T, and λ_0 represent the energy activation barrier, Boltzmann's constant, absolute interface temperature, and effective attempt frequency prefactor (based on atomic vibrations [124]), respectively. Applying equation (3) to the plot of ln (λ) against (1/T) gives the E_a/k as the slope as shown by Raghuraman *et al.* [115].

Equation (4) is used to describe the change in the oxygen concentration during a linear temperature ramp [125].

$$\frac{df}{dT} = \frac{v}{\beta}f^n e^{-(E_a - \emptyset(F_N))/kT}, \tag{4}$$

where v, β, f, n, F_N, and T are the exponential prefactor, rate of temperature ramp, the measured friction (which correlates linearly with the concentration of oxygen), reaction order, applied normal tip force, and the absolute interface temperature, respectively. $\phi(F_N)$ explains the effect of applied force on the energy outlook and relies on the geometry of the under-study molecule and the location and direction of the applied forces. When the temperature increases linearly at a steady load, the energy barrier is considered as a constant. The energy barrier (E_{eff}) includes the influence of the applied force (*i.e.* $E_{eff} = E_a - \phi(F_N)$). Integrating equation (4) over temperature at constant force gives equation (5) which is similar to the established solution for bulk thermal study and effective estimation as expressed by Coats and Redfern [125].

$$Q = \frac{v}{\beta}e^{-E_{eff}/kT}\left(\frac{k}{E_{eff}}\right)\left[1 - \left(\frac{kT}{E_{eff}}\right)\right]. \tag{5}$$

For a first-order reaction, the plot of ln(Q) against 1/T gives a straight line with the slope showing a direct relationship with activation energy (E_a) as shown in Figure 4(m).

Furthermore, it should be noted that an increasing rate of bond disengagement under the influence of external force was first proposed by Bell [126]. However, above certain applied forces, Bell's model cannot account for the nonlinear stress dependency and the loss of the reaction pathway. So, as seen in Figure 4(p), Raghuraman *et al.* [115] adopted Bell's model extension with a second-order correction (equation (6)) to fit the plot of the E_a against F_N revealing the existence of the Harmond effect as previously discussed.

$$E_{eff} = E_a - \Delta x F_N + \frac{\Delta\chi}{2}F_N^2. \tag{6}$$

where Δx and ΔX are the distance between reactants and the change in mechanical compliance, respectively.

5 Tip-induced strain for optimizing the optoelectronic properties

The high stretchability property of 2D materials especially TMDC makes it feasible to tune their optical and electronic properties *via* external strain inducement [127,128]. This interesting phenomenon has been explored in the field of strain engineering where materials' physical properties are altered by manipulating the applied elastic strain fields [127,129]. For instance, single-layer MoS_2 can go through a direct-to-indirect bandgap transition at ~2% uniaxial

tensile strain and a semiconducting-to-metal transition at 10–15% biaxial tensile strain [130,131]. This large bandgap sensitivity (from 1.8 to 0 eV) is practically exploited in MoS_2 and other TMDC because they are capable of undergoing a high level of strain without rupture [132]. Over the years, different straining techniques such as bending and elongation of a flexible substrate [133,134], piezoelectric stretching [135], exploiting the thermal expansion mismatch [136], and controlled wrinkling [137] have been adopted for strain inducement. However, in recent years, AFM tip has been considered one of the most effective methods of inducing and exploring strain-induced electronic properties at the nanoscale. Since, when the AFM tip is pressed against the film, it can generate a high stress concentration and a large strain gradient [138].

Chaudhary *et al.* used conductive AFM probes to apply force on layered MoS_2 junctions in order to observe the modulation of current transport behavior under mechanical stress as shown in Figure 5(a and b) [139]. They demonstrated that both strain and strain gradient are very useful in the modification of the MoS_2 band structure, permitting resistance tuning up to 4 orders of magnitude. Using the Hertzian contact model [140], they showed that extrinsic factors like changes in tip-sample contact geometry and sample thickness are not the dominant cause of the observed changes in transport behavior. However, the change in the transport behavior is majorly due to the intrinsic factors related to the modification of the MoS_2 band structure and barrier profile. These findings provide valuable insights into the underlying mechanisms of mechanical stress-induced modulation of transport behavior in 2D materials and have potential implications for the development of novel nanoelectronic devices. Moreover, they showed the existence of a tip-induced flexoelectric effect (Figure 5(c and d)), where an obvious shift of the photocurrent onset with increasing tip load was observed. Interestingly, the study of the flexoelectric effect has recently gained significant attention due to its potential applications in various fields such as energy conversion [141], data storage [142], and energy harvesting [143]. The effect refers to the conversion of mechanical stress into electrical polarization in materials, and its magnitude is proportional to the strength of the strain gradient [144,145]. An AFM tip can apply mechanical stress to a material, creating a strain gradient that triggers a flexoelectric response. By measuring the electrical response of the material, researchers can study the relationship between the strength of the strain gradient and the magnitude of the flexoelectric effect [146].

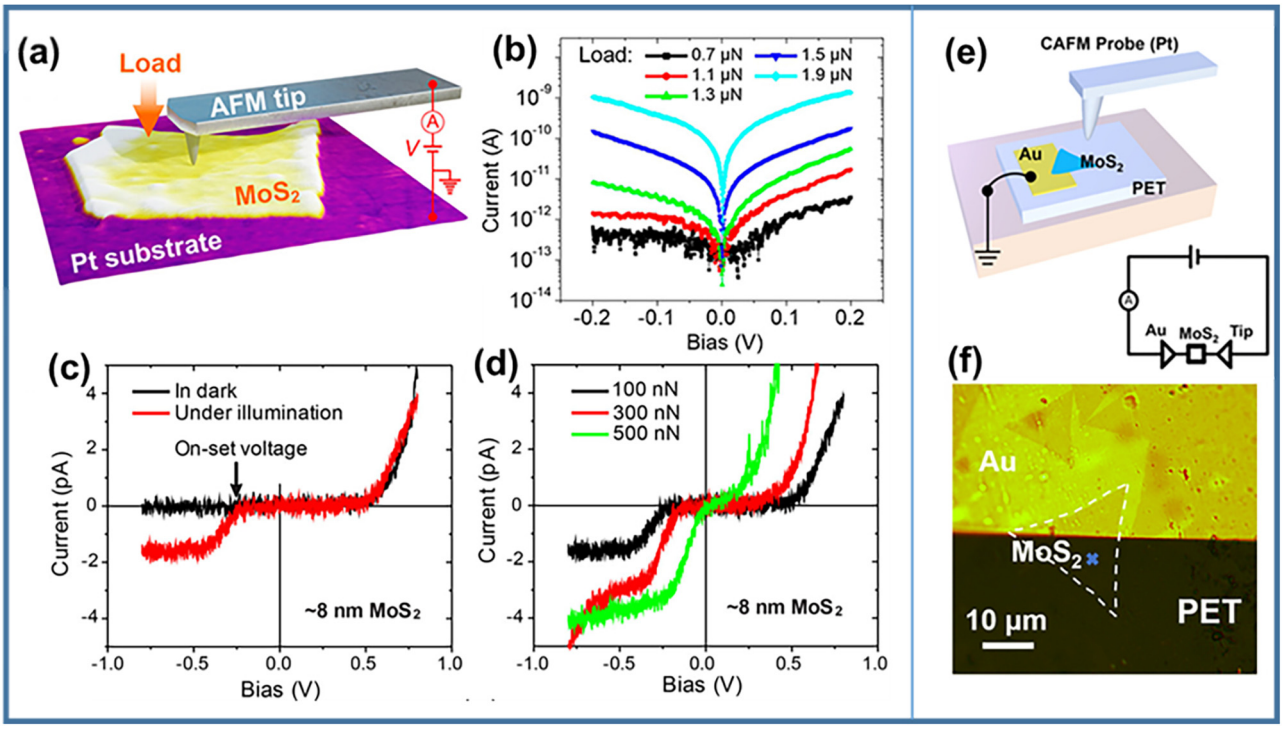

Figure 5: (a) Schematic representation of the experimental setup; an AFM probe is placed on the MoS_2 to permit transport measurements across the thickness of the MoS_2. (b) Plots showing the Current–Voltage characteristics under varying tip loading. I–V plots obtained in the dark and under illumination (c) at 50 nm minimum load and (d) for varying tip loads [139]. (e) Schematic illustration of out-plane strain loading by conductive-AFM. Inset is the experimental circuit schematic. (f) Microscopic picture of a typical monolayer MoS_2 on PET [147].

The application of gradient mechanical stress to MoS_2 junctions has been shown not only to induce changes in their transport properties but also have the potential to enhance the photoresponse performance of MoS_2 photodetectors. The impact of mechanical strain on the photoresponse performance of MoS_2 photodetectors is challenging to quantify due to the changing effective luminescent area as strain increases, resulting in uncertainties in quantifying photovoltaic performance parameters. Feng *et al.* employed a flexible PET base to separate the MoS_2 end under stress from the end in contact with the metal electrode to address this issue. Their experimental setup (Figure 5(e and f)) confines the stress applied to the tip of the probe and enables accurate determination of the area of light illumination [147]. The optoelectronic performance of MoS_2 is dependent on contact area and Schottky barrier height, both of which are affected by mechanical strain. The flexible polarization field can effectively modulate the carrier distribution and interfacial barrier, leading to an increase in the local electron affinity of MoS_2, thereby facilitating the transport of photogenerated carriers in the device. These findings suggest that the flexural electric effect can enhance the optoelectronic performance of MoS_2 by modulating the Schottky barrier.

Pu *et al.* [148] examined the flexoelectricity-improved photovoltaic effect in Gr/Si Schottky Junction (GSJ). They used the AFM tip to apply different loads generating a strain gradient in the junction, thereby accessing the GSJ current response. They proved an increment in the open-circuit voltage (V_{oc}) and Schottky barrier height when the laser is switched on. This development can lead to a 20% improvement in the GSJ power conversion efficiency. Besides MoS_2 and graphene, Wu and co-workers had earlier proved that the bandgap of few-layered black phosphorus (BP) can be effectively decreased *via* out-of-plane compressive strain using AFM tip, leading to dramatic modulation of the vertical electrical performance of the BP and further effecting a nonlinear current–voltage curve to linear current–voltage curve transition [149].

6 Tip-based cleaning and smoothening of 2D materials heterostructures

In recent years, 2D materials and their heterostructures have garnered widespread attention in applied physics and optoelectronic devices due to their exceptional properties. However, during the fabrication process, mechanical exfoliation is commonly used. Despite its ability to produce high-quality 2D materials, the transfer and stacking processes often introduce impurities and contaminants. For instance, commonly used sacrificial organic interlayers can leave organic residues that affect the surface purity and performance of the 2D materials. Environmental contaminants like dust and moisture can also adhere to the material surface during transfer, leading to degraded heterostructure performance. These impurities and contaminants significantly impact the performance of 2D material heterostructures. For example, residues can decrease electrical performance, reduce charge mobility, alter optical properties, and decrease chemical stability. Therefore, effectively removing these impurities to ensure the high quality and performance of heterostructures is a critical research focus.

During the transfer process, PMMA serves merely as a supporting material, and its removal is exceedingly challenging. Residual PMMA can significantly alter the intrinsic properties of graphene. Consequently, researchers have developed various methods to remove PMMA residues from the graphene surface, including thermal annealing [150–154], plasma treatment [155–159], electron beam treatment [160,161], and ion beam treatment [162,163]. Besides external cleaning processes, Hou *et al.* demonstrated that vdW heterostuctures can undergo self-cleaning [164]. Although these cleaning methods are effective to some extent, completely eliminating PMMA residues from the graphene surface at the nanoscale remains a major challenge. Further optimization of these techniques and the exploration of new methods are crucial to ensure the purity of graphene and maintain its superior properties. A recent review from Dong *et al.* [165] discussed the different 2D transfer methods, sources of contaminants, and cleaning processes and Ma *et al.* [166] demonstrated the behavior of liquids trapped at the interface of 2D materials using the AFM technique. So this section will focus on the use of AFM as a cleaning and interface properties optimization tool for 2D materials.

Researchers have effectively used AFM tips to mechanically remove polymer residues from graphene surfaces without the need for additional chemicals which might otherwise contaminate the surface [167–170]. Their primarily focus was on residues and contaminants on the graphene surface and improving the surface properties of graphene. However, the presence of wrinkles, grain boundaries, and trapped molecules under the layer can also significantly affect the consistency and homogeneity of 2D material interfaces [171]. Rosenberger *et al.* [172] investigated the use of AFM to create clean and homogeneous interfaces in 2D material heterostructures. As seen

in Figure 6(a and b), by applying a normal force to the 2D layer, the AFM tip squeezes out contaminants trapped between the layer and the substrate. This process enhances the spatial homogeneity of PL tests and decreases the PL line widths. Furthermore, the technique improves interlayer coupling in 2D materials heterostructures, as evidenced by the observation of interlayer excitons. In heterostructures such as $MoSe_2$–WSe_2, the technique enabled strong interlayer exciton emission and bilayer-like Raman spectrum, indicating enhanced interlayer interaction, as shown in Figure 6(c). Palai *et al.* [173] explored the use of AFM contact mode to improve the interface quality of TMD heterostructures. They investigate the moiré properties of the materials, as illustrated by the AFM morphology images before and after treatment shown in Figure 6(d). The improved interface quality led to enhanced moiré effects, as evidenced by the observation of stronger interlayer exciton emissions, shown in Figure 6(e). Ding *et al.* [174,175] demonstrated that nano-spherical AFM probes are highly effective for cleaning and improving the quality of 2D van der Waals heterostructures. These probes offer significant advantages over traditional pyramid probes, including reduced mechanical damage, improved cleaning efficiency, and enhanced material properties. The result of the surface potential of regions cleaned with the nano-spherical probe was more consistent and exhibited less deviation compared to those cleaned with the pyramid probe, as shown in Figure 6(f).

Researchers have combined AFM flattening with other tools and processes to better understand the distribution state of contaminants as a way of performing predictive advance removal of contaminants trapped under the 2D materials layer. As proposed by Schwartz *et al.* [176], a combination of AFM flattening and photothermally induced resonance (PTIR) techniques were effectively employed to obtain infrared spectra and maps of contaminants down to a few

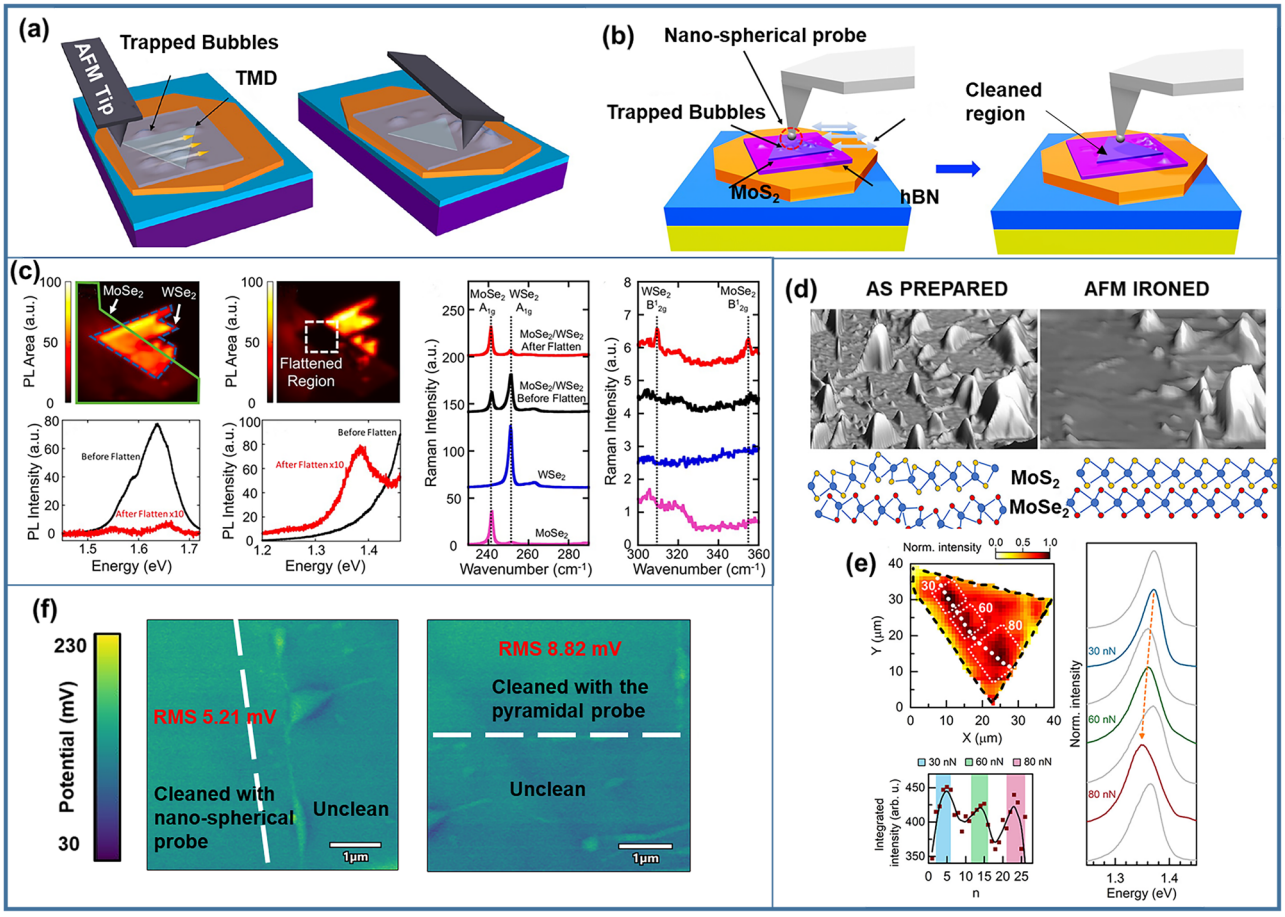

Figure 6: (a) and (b) Cartoon illustration of the AFM cleaning process [172,174]. (c) The PL quenching effect images before and after AFM treatment, are shown for stronger interlayer interactions [172]. (d) AFM topography images before and after ironing [173]. (e) The image of interlayer exciton emissions and strain of PL peak positions under different applied forces [173]. (f) The surface potential images of the region were cleaned with the nano-spherical probe and cleaned with the pyramid probe [174].

attomoles at nanometer-scale resolution (Figure 7(a)). The combination of PTIR for identifying contaminants (Figure 7(b)) and the *nano squeegee* technique for their removal provides a robust approach for improving vdWH fabrication processes, leading to cleaner and more intrinsic heterostructures. Kim *et al.* proposed a reliable approach to optimize fully completed vdWHs devices by direct post-processing surface treatment based on thermal annealing and contact mode AFM as shown in Figure 7(c) [177]. The combination of thermal annealing and AFM cleaning provides a robust approach to significantly improve the quality of van der Waals heterostructures. The study includes detailed magnetotransport measurements before and after AFM treatment on graphene and MoS_2 devices. From Figure 7(d), the results indicate notable improvements in Shubnikov-de Haas oscillations and the overall electronic quality of the devices. By addressing random strain fluctuations and removing residual contaminants, these postprocessing methods enable the achievement of uniform intrinsic properties in 2D material devices. The study highlights the importance of such techniques in advancing the fabrication and application of high-performance 2D heterostructures. Talha-Dean et al. used thermal scanning probes to fabricate clean interfaces in vdW heterostructures as described in Figure 7(e) [178]. This method combines thermal annealing and mechanical tip-based cleaning to effectively reduce interface disorder. The study demonstrates a transition from macroscopic current flow to single-electron tunneling, which is crucial for quantum information processing and quantum sensing applications. Electrical transport measurements at cryogenic temperatures show substantial improvements in device performance after cleaning (Figure 7(f)). Chen *et al.* [179] demonstrated the enhancement of the electrical properties of MoS_2 devices using AFM contact mode cleaning of hBN-encapsulated monolayer MoS_2 transistors (Figure 7(g)). They compared the properties of as-transferred heterostructures and transistors before and after AFM tip-based cleaning using back-gated field-effect measurements. The extrinsic mobility of monolayer MoS_2 field-effect transistors increased from 21 cm^2/Vs before cleaning to 38 cm^2/Vs after cleaning, as seen in Figure 7(h).

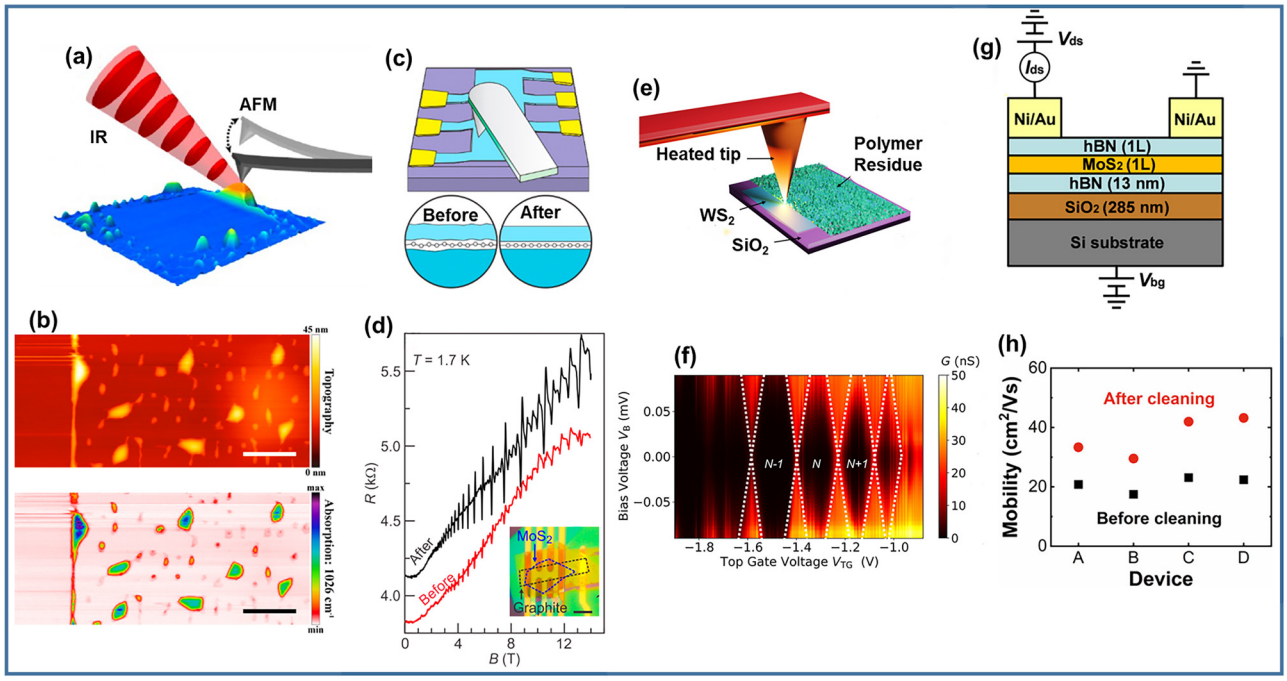

Figure 7: (a) Schematic illustrating PTIR measurements [176]. (b) PTIR absorption imaging reveals the nano contaminant distribution within vdWHs [176]. (c) Schematic of the van der Waals heterostructure device geometry and the AFM treatment [177]. (d) Shubnikov–de Haas oscillations on device M1 with a density of 5×10^{12} cm^{-2} at $T = 1.7$ K. Red and black lines show results of before and after contact mode AFM, respectively [177]. (e) Schematic of the heated AFM probe cleaning process [178]. (f) Charge stability image showing diamond-shaped regions of suppressed conductance suggesting Coulomb blockade at $V_{BG} = 3.7$ V. The diamond sizes increase with more negative V_{TG} due to a reduction in quantum dot size with stronger electrostatic confinement [178]. (g) Cross-sectional outlook of the field effect transistors (FETs), together with the electrical connections to characterize the devices [179]. (h) Extrinsic mobilities of the FETs before and after tip-based cleaning [179].

7 Outlook/Conclusion

This review has discussed several intriguing AFM tip-based methods used in the study and design of 2D materials and devices, showcasing innovative ways to locally adjust these materials' chemical and physical properties at the nanoscale. These techniques open up vast possibilities for 2D materials research with AFM. However, despite these advancements, there is still a need for substantial improvements in current AFM technology. Firstly, attaching 2D materials to an AFM tip remains a complex challenge, as the sharpness of the AFM tip can create stress concentrations that may cause the 2D material to tear. Additionally, the various attachment methods reviewed often result in partial amorphization and rough bonding, likely due to the tip's roughness or damaged structure, which can significantly impact the accuracy of the results. Furthermore, issues such as lack of repeatability and control over the number of layers transferred to the tip still persist. Consequently, more intensive research is necessary to address these challenges. One promising solution is the use of specialized tips, such as the new nano-spherical tip with ~0.2 nm roughness [28,180,181]), which could facilitate the attachment of smooth and crystalline 2D materials, thereby ensuring a more homogeneous and intimate interface for nanotribology studies.

Second, studying twist-angle-dependent properties of 2D materials requires extremely high precision and uniformity in controlling the rotation, as even small variations in the twist angle can significantly impact the material's properties. Current AFM setups are not designed for precise rotational control, and relying on manual rotation, as described in Section 3, can introduce inaccuracies. Additionally, there is a higher risk of inducing strain, misalignment, tearing, wrinkling, or delamination during AFM tip rotation due to the fragile nature of 2D materials. Reproducing the same twist angle configuration and measurements is also challenging because of varying factors such as tip interactions, adhesion, and material sensitivity, making it difficult to achieve consistent results. Therefore, careful experimental design and further advancements in AFM technology are necessary to address these issues. Also, it is important to note that the experimental demonstrations of twist-angle tunable devices reviewed in this work primarily focused on MoS_2/graphene and hBN/graphene/hBN heterostructures. However, the techniques discussed are broadly applicable and can be extended to other 2D material heterostructures, potentially paving the way for a new class of experiments to explore twist-angle-dependent phenomena. This is especially important as 2D materials are poised to enable the development of a wide range of electronic devices such as transistors, diodes, photodetectors, memristors, *etc.* [182–186] that could drive the post-Moore electronics era [187–189]. Additionally, given that the AFM tip has demonstrated the ability to disassemble nanoparticles and reposition them at a specific location, adapting this technique for 2D material transfer could spark significant interest in the scientific community. Such an approach would greatly simplify the currently complex, multi-step processes involved in transferring 2D materials.

Thirdly, while AFM can induce local changes in the surface chemistry of 2D materials, it remains challenging to precisely control the magnitude of these changes, the outcomes of the reactions, and their reproducibility. This difficulty arises from the sensitivity of the process to small variations in surface topography, tip contamination, environmental factors, and electronic bonding configurations, all of which can influence reactivity. Moreover, the reaction mechanisms at the nanoscale are still not fully understood. Further studies are needed to address the above challenges. Also, employing accurate theoretical models and simulations such as MD [190–192], and DFT [193–196] will complement the experimental study to provide a comprehensive understanding of the contact mechanics, reaction pathways, and the products' stoichiometry. For instance, DFT has been successfully applied to investigate the oxygen reduction mechanism of doped graphene [197] and determined the relation between the surface stress, the resulting strain, and the thickness of 2D layered material [198]. Furthermore, the surface chemistry modifications discussed in this review have primarily focused on graphene, suggesting a new direction for research into the tip-based modifications of other functionalized 2D materials [199,200].

Fourthly, regarding the use of AFM tips for strain engineering, it is still challenging to precisely control the exact magnitude and direction of the applied strain. Small variations in the tip-sample interaction like the contact force, angle, or tip geometry can affect the intended results. Furthermore, applying excessive strain or uneven strain distribution can induce defects such as cracks, wrinkles, or dislocations resulting in reduced material performance. These defects could lead to degradation in materials properties. Since tip-induced strain can alter the lattice structure and the electronic band, it may also unintentionally introduce localized charge traps or scattering centers, further reducing device performance. Consequently, additional research is required to optimize this process and improve device performance.

Fifthly, while AFM can effectively remove bubbles and contaminants from the interfaces of 2D materials, care

must be taken to prevent unintentional changes to the surface chemistry during the cleaning process. Additionally, localized structural damage, such as wrinkles or dislocations, may be introduced, potentially compromising the electronic and mechanical properties of the vdW heterostructure devices. The sharp AFM tip is also prone to wear, which can lead to a loss of resolution and precision. Furthermore, the AFM tip may pick up material from the surface and redeposit it elsewhere, causing recontamination and reducing the effectiveness of the cleaning and smoothing processes. Therefore, careful experimental design and customized tips are required to address these problems.

In conclusion, most of the techniques discussed in this review are effective for small-scale studies, but scaling them up for industrial or practical applications remains challenging. For example, AFM can modify surface chemistry at very small scales (from nanometers to a few micrometers), but achieving large-scale, uniform surface chemistry modifications is difficult. Similarly, AFM tip-induced strain is highly localized, typically affecting only a small area of the material. However, applying strain uniformly over larger areas is often necessary for optimizing optoelectronic properties, which is difficult with current AFM setups. Additionally, cleaning and smoothing devices with AFM usually requires scanning the surface at slow speeds to maintain precise control over tip interactions, making the process time-consuming and challenging to achieve uniformity across larger areas. Given the increasing demand for efficient vdW heterostructure devices, there is a pressing need for scalable, high-throughput, and standardized methods for cleaning and smoothing these materials. Therefore, the techniques discussed in this article can support research in 2D materials. They have provided meaningful insights that can guide future research in developing scalable, high-throughput, and cost-effective technologies for industrial applications.

Funding information: This work was supported by the Haining City government Chaoyang Funds and National Key Research and Development Program projects (2022YFB3203600).

Author contributions: Paul C. Uzoma and Xiaolei Ding: literature review, writing – original draft, visualization, review, and editing. Baoshi Qiao and Emeka E. Oguzie: writing – review, and editing. Yang Xu and Xiaorui Zheng: methodology, writing – review, and editing. Huan Hu: conceptualization, project administration, and supervision. All authors have accepted responsibility for the entire content of this manuscript and approved its submission.

Conflict of interest: The authors state no conflict of interest.

Data availability statement: All data generated or analysed during this study are included in this published article.

References

[1] Novoselov KS, Geim AK, Morozov SV, Jiang D, Zhang Y, Dubonos SV, et al. Electric field effect in atomically thin carbon films. Science. 2004;306(5696):666–9.

[2] Mounet N, Gibertini M, Schwaller P, Campi D, Merkys A, Marrazzo A, et al. Two-dimensional materials from high-throughput computational exfoliation of experimentally known compounds. Nat Nanotechnol. 2018;13(3):246–52.

[3] Wang F, Wang Z, Wang Q, Wang F, Yin L, Xu K, et al. Synthesis, properties, and applications of 2D non-graphene materials. Nanotechnology. 2015;26(29):292001.

[4] Uzoma PC, Hu H, Khadem M, Penkov OV. Tribology of 2D Nanomaterials: A review. Coatings. 2020;10(9):897.

[5] Shanmugam V, Mensah RA, Babu K, Gawusu S, Chanda A, Tu YM, et al. A Review of the synthesis, properties, and applications of 2D materials. Part Part Syst Char. 2022;39(6):2200031.

[6] Fiori G, Bonaccorso F, Iannaccone G, Palacios T, Neumaier D, Seabaugh A, et al. Electronics based on two-dimensional materials. Nat Nanotechnol. 2014;9(10):768–79.

[7] Li Z, Xu K, Wei F. Recent progress in photodetectors based on low-dimensional nanomaterials. Nanotechnol Rev. 2018;7(5):393–411.

[8] Wu Y, Wang Y, Bao D, Deng X, Zhang S, Yu-chun L, et al. Emerging probing perspective of two-dimensional materials physics: terahertz emission spectroscopy. Light Sci Appl. 2024;13(1):146.

[9] Ho P. Twenty years of 2D materials. Nat Phys. 2024;20(1):1.

[10] Yadav A, Acosta CM, Dalpian GM, Malyi OI. First-principles investigations of 2D materials: Challenges and best practices. Matter. 2023;6(9):2711–34.

[11] Dai Z, Lu N, Liechti KM, Huang R. Mechanics at the interfaces of 2D materials: Challenges and opportunities. Curr Opin Solid State Mater Sci. 2020;24(4):100837.

[12] Binnig G, Quate CF, Gerber C. Atomic force microscope. Phys Rev Lett. 1986;56(9):930–3.

[13] Bhushan B, Marti O. Scanning Probe Microscopy — Principle of operation, instrumentation and probes. In: Bhushan B, editor. Springer handbook of nanotechnology. Berlin, Heidelberg: Springer Berlin Heidelberg; 2017. p. 725–68.

[14] Brotons-Alcázar I, Terreblanche JS, Giménez-Santamarina S, Gutiérrez-Finol GM, Ryder KS, Forment-Aliaga A, et al. Atomic force microscopy beyond topography: Chemical sensing of 2D material surfaces through adhesion measurements. ACS Appl Mater Interfaces. 2024;16(15):19711–9.

[15] Bhushan B, Israelachvili JN, Landman U. Nanotribology: friction, wear and lubrication at the atomic scale. Nature. 1995;374(6523):607–16.

[16] Bhushan B, Dandavate C. Thin-film friction and adhesion studies using atomic force microscopy. J Appl Phys. 2000;87(3):1201–10.

[17] Gao Y, Kim S, Zhou S, Chiu H-C, Nélias D, Berger C, et al. Elastic coupling between layers in two-dimensional materials. Nat Mater. 2015;14(7):714–20.

[18] Li J, Zhang G, Wang L, Dai Z. Indentation of a plate on a thin transversely isotropic elastic layer. Acta Mech Solida Sin. 2024.

[19] Khan RM, Rejhon M, Li Y, Parashar N, Riedo E, Wixom RR, et al. Probing the mechanical properties of 2D materials via atomic-force-microscopy-based modulated nanoindentation. Small Methods. 2024;8(3):2301043.
[20] Dai Z, Lu N. Poking and bulging of suspended thin sheets: Slippage, instabilities, and metrology. J Mech Phys Solids. 2021;149:104320.
[21] Garrido M, Naranjo A, Pérez EM. Characterization of emerging 2D materials after chemical functionalization. Chem Sci. 2024;15(10):3428–45.
[22] Sheehan PE, Lieber CM. Friction between van der Waals solids during lattice directed sliding. Nano Lett. 2017;17(7):4116–21.
[23] Carpick RW, Salmeron M. Scratching the Surface: Fundamental investigations of tribology with atomic force microscopy. Chem Rev. 1997;97(4):1163–94.
[24] Balakrishna SG, de Wijn AS, Bennewitz R. Preferential sliding directions on graphite. Phys Rev B. 2014;89(24):245440.
[25] Yu C, Dai Z. Premature jump-to-contact with elastic surfaces. J Mech Phys Solids. 2024;193:105919.
[26] Yu C, Zeng W, Wang B, Cui X, Gao Z, Yin J, et al. Stiffer is stickier: Adhesion in elastic nanofilms. Nano Lett. 2024;25(5):1876–82.
[27] Felts JR, Oyer AJ, Hernández SC, Whitener Jr KE, Robinson JT, Walton SG, et al. Direct mechanochemical cleavage of functional groups from graphene. Nat Commun. 2015;6(1):6467.
[28] Uzoma PC, Ding X, Wen X, Zhang L, Penkov OV, Hu H. A wear-resistant silicon nano-spherical AFM probe for robust nanotribological studies. Phys Chem Chem Phys. 2022;24(38):23849–57.
[29] Gnecco E, Bennewitz R, Gyalog T, Loppacher C, Bammerlin M, Meyer E, et al. Velocity dependence of atomic friction. Phys Rev Lett. 2000;84(6):1172–5.
[30] Park JY, Salmeron M. Fundamental aspects of energy dissipation in friction. Chem Rev. 2014;114(1):677–711.
[31] Lantz MA, O'Shea SJ, Hoole ACF. Welland MEJAPL. Lateral stiffness of the tip and tip-sample contact in frictional force microscopy. Appl Phys Lett. 1997;70(8):970–2.
[32] Rejhon M, Lavini F, Khosravi A, Shestopalov M, Kunc J, Tosatti E, et al. Relation between interfacial shear and friction force in 2D materials. Nat Nanotechnol. 2022;17(12):1280–7.
[33] Eigler DM, Schweizer EK. Positioning single atoms with a scanning tunnelling microscope. Nature. 1990;344(6266):524–6.
[34] Giessibl FJ. Probing the nature of chemical bonds by atomic force microscopy. Molecules. 2021;26(13):4068.
[35] Han XH, Huang ZH, Fan P, Zhu SY, Shen CM, Chen H, et al. Research progress of surface atomic manipulation and physical property regulation of low-dimensional structures. Acta Phys Sin. 2022;71(12):128102.
[36] Craciun AD, Donnio B, Gallani JL, Rastei MV. High-resolution manipulation of gold nanorods with an atomic force microscope. Nanotechnology. 2020;31(8):085302.
[37] Li M, Xun K, Zhu X, Liu D, Liu X, Jin X, et al. Research on AFM tip-related nanofabrication of two-dimensional materials. Nanotechnol Rev. 2023;12(1):20230153.
[38] Wu S, Gu J, Li R, Tang Y, Gao L, An C, et al. Progress on mechanical and tribological characterization of 2D materials by AFM force spectroscopy. Friction. 2024;12(12):2627–56.
[39] Wu F-B, Zhou S-J, Ouyang J-H, Wang S-Q, Chen L. Structural superlubricity of two-dimensional materials: Mechanisms, properties, influencing factors, and applications. Lubricants. 2024;12(4):138.
[40] Li Y, Lin B, Ge L, Guo H, Chen X, Lu M. Real-time spectroscopic monitoring of photocatalytic activity promoted by graphene in a microfluidic reactor. Sci Rep. 2016;6(1):28803.
[41] Hu G, Ou Q, Si G, Wu Y, Wu J, Dai Z, et al. Topological polaritons and photonic magic angles in twisted α-MoO_3 bilayers. Nature. 2020;582(7811):209–13.
[42] Wang H, Dong C, Gui Y, Ye J, Altaleb S, Thomaschewski M, et al. Self-powered Sb_2Te_3/MoS_2 heterojunction broadband photodetector on flexible substrate from visible to near infrared. Nanomaterials. 2023;13(13):1973.
[43] Koo JH, Yun H, Lee W, Sunwoo S-H, Shim HJ, Kim D-H. Recent advances in soft electronic materials for intrinsically stretchable optoelectronic systems. Opto-Electron Adv. 2022;5(8):210131.
[44] Rosenkranz A, Righi MC, Sumant AV, Anasori B, Mochalin VN. Perspectives of 2D MXene tribology. Adv Mater. 2023;35(5):2207757.
[45] Marian M, Berman D, Rota A, Jackson RL, Rosenkranz A. Layered 2D nanomaterials to tailor friction and wear in machine elements – A review. Adv Mater Interfaces. 2022;9(3):2101622.
[46] Hui F, Vajha P, Shi Y, Ji Y, Duan H, Padovani A, et al. Moving graphene devices from lab to market: advanced graphene-coated nanoprobes. Nanoscale. 2016;8(16):8466–73.
[47] Wen Y, Chen J, Guo Y, Wu B, Yu G, Liu Y. Multilayer graphene-coated atomic force microscopy tips for molecular junctions. Adv Mater. 2012;24(26):3482–5.
[48] Lanza M, Bayerl A, Gao T, Porti M, Nafria M, Jing GY, et al. Graphene-coated atomic force microscope tips for reliable nanoscale electrical characterization. Adv Mater. 2013;25(10):1440–4.
[49] Yu K, Xu P, Peng Y, Huang Y, Lang H, Ding S. Ultra-low friction and stiffness dependence of interlayer friction in graphite flakes under various rotation angles. Mater Today Adv. 2023;18:100380.
[50] Liu S-W, Wang H-P, Xu Q, Ma T-B, Yu G, Zhang C, et al. Robust microscale superlubricity under high contact pressure enabled by graphene-coated microsphere. Nat Commun. 2017;8(1):14029.
[51] Yuan Y, Weber J, Li J, Tian B, Ma Y, Zhang X, et al. On the quality of commercial chemical vapour deposited hexagonal boron nitride. Nat Commun. 2024;15(1):4518.
[52] Nakatani M, Fukamachi S, Solís-Fernández P, Honda S, Kawahara K, Tsuji Y, et al. Ready-to-transfer two-dimensional materials using tunable adhesive force tapes. Nat Electron. 2024;7(2):119–30.
[53] Tian J, Yin X, Li J, Qi W, Huang P, Chen X, et al. Tribo-induced interfacial material transfer of an atomic force microscopy probe assisting superlubricity in a WS2/Graphene heterojunction. ACS Appl Mater Interfaces. 2020;12(3):4031–40.
[54] Liu Y, Song A, Xu Z, Zong R, Zhang J, Yang W, et al. Interlayer friction and superlubricity in single-crystalline contact enabled by two-dimensional flake-wrapped atomic force microscope tips. ACS Nano. 2018;12(8):7638–46.
[55] Leven I, Krepel D, Shemesh O, Hod O. Robust Superlubricity in graphene/h-BN heterojunctions. J Phys Chem Lett. 2013;4(1):115–20.
[56] Bowden FP, Tabor D. The friction and lubrication of solids. Oxford, United Kingdom: Oxford University Press; 1964.
[57] Gyalog T, Gnecco E, Meyer E. Fundamentals of friction and wear. In: Gnecco E, Meyer E, editors. NanoScience and technology. 1st edn. Heidelberg: Springer Berlin; 2007. p. 716.
[58] Carr S, Massatt D, Fang S, Cazeaux P, Luskin M, Kaxiras E. Twistronics: Manipulating the electronic properties of two-

dimensional layered structures through their twist angle. Phys Rev B. 2017;95(7):075420.
[59] Zhou R, Habib M, Iqbal MF, Hussain N, Farooq S, Haleem YA, et al. Twisto-photonics in two-dimensional materials: A comprehensive review. Nanotechnol Rev. 2024;13(1):20240086.
[60] Kim H, Kim C, Jung Y, Kim N, Son J, Lee G-H. In-plane anisotropic two-dimensional materials for twistronics. Nanotechnology. 2024;35(26):262501.
[61] Hou Y, Zhou J, Xue M, Yu M, Han Y, Zhang Z, et al. Strain engineering of twisted bilayer graphene: The rise of strain-twistronics. Small. 2024;2311185.
[62] Cao Y, Fatemi V, Fang S, Watanabe K, Taniguchi T, Kaxiras E, et al. Unconventional superconductivity in magic-angle graphene superlattices. Nature. 2018;556(7699):43–50.
[63] Chen G, Sharpe AL, Gallagher P, Rosen IT, Fox EJ, Jiang L, et al. Signatures of tunable superconductivity in a trilayer graphene moiré superlattice. Nature. 2019;572(7768):215–9.
[64] Alexeev EM, Ruiz-Tijerina DA, Danovich M, Hamer MJ, Terry DJ, Nayak PK, et al. Resonantly hybridized excitons in moiré superlattices in van der Waals heterostructures. Nature. 2019;567(7746):81–6.
[65] Rivera P, Schaibley JR, Jones AM, Ross JS, Wu S, Aivazian G, et al. Observation of long-lived interlayer excitons in monolayer $MoSe_2$–WSe_2 heterostructures. Nat Commun. 2015;6(1):6242.
[66] Jin C, Regan EC, Yan A, Iqbal Bakti Utama M, Wang D, Zhao S, et al. Observation of moiré excitons in WSe_2/WS_2 heterostructure superlattices. Nature. 2019;567(7746):76–80.
[67] Sharpe AL, Fox EJ, Barnard AW, Finney J, Watanabe K, Taniguchi T, et al. Emergent ferromagnetism near three-quarters filling in twisted bilayer graphene. Science. 2019;365(6453):605–8.
[68] Gonzalez-Arraga LA, Lado JL, Guinea F, San-Jose P. Electrically controllable magnetism in twisted bilayer graphene. Phys Rev Lett. 2017;119(10):107201.
[69] Spanton EM, Zibrov AA, Zhou H, Taniguchi T, Watanabe K, Zaletel MP, et al. Observation of fractional Chern insulators in a van der Waals heterostructure. Science. 2018;360(6384):62–6.
[70] Decker R, Wang Y, Brar VW, Regan W, Tsai H-Z, Wu Q, et al. Local electronic properties of graphene on a BN substrate via scanning tunneling microscopy. Nano Lett. 2011;11(6):2291–5.
[71] Yankowitz M, Xue J, Cormode D, Sanchez-Yamagishi JD, Watanabe K, Taniguchi T, et al. Emergence of superlattice Dirac points in graphene on hexagonal boron nitride. Nat Phys. 2012;8(5):382–6.
[72] Hunt B, Sanchez-Yamagishi JD, Young AF, Yankowitz M, LeRoy BJ, Watanabe K, et al. Massive Dirac fermions and Hofstadter butterfly in a van der Waals heterostructure. Science. 2013;340(6139):1427–30.
[73] Ponomarenko LA, Gorbachev RV, Yu GL, Elias DC, Jalil R, Patel AA, et al. Cloning of Dirac fermions in graphene superlattices. Nature. 2013;497(7451):594–7.
[74] Dean CR, Wang L, Maher P, Forsythe C, Ghahari F, Gao Y, et al. Hofstadter's butterfly and the fractal quantum Hall effect in moiré superlattices. Nature. 2013;497(7451):598–602.
[75] Kim K, Yankowitz M, Fallahazad B, Kang S, Movva HCP, Huang S, et al. van der Waals heterostructures with high accuracy rotational alignment. Nano Lett. 2016;16(3):1989–95.
[76] Jat MK, Tiwari P, Bajaj R, Shitut I, Mandal S, Watanabe K, et al. Higher order gaps in the renormalized band structure of doubly aligned hBN/bilayer graphene moiré superlattice. Nat Commun. 2024;15(1):2335.
[77] Wang D, Chen G, Li C, Cheng M, Yang W, Wu S, et al. thermally induced graphene rotation on hexagonal Boron Nitride. Phys Rev Lett. 2016;116(12):126101.
[78] Chari T, Ribeiro-Palau R, Dean CR, Shepard K. Resistivity of rotated graphite–graphene contacts. Nano Lett. 2016;16(7):4477–82.
[79] Du L, Yu H, Liao M, Wang S, Xie L, Lu X, et al. Modulating PL and electronic structures of MoS_2/graphene heterostructures via interlayer twisting angle. Appl Phys Lett. 2017;111(26):263106.
[80] Yuan J, Liao M, Huang Z, Tian J, Chu Y, Du L, et al. Precisely controlling the twist angle of epitaxial MoS_2/graphene heterostructure by AFM tip manipulation. Chin Phys B. 2022;31(8):087302.
[81] Ribeiro-Palau R, Zhang C, Watanabe K, Taniguchi T, Hone J, Dean CR. Twistable electronics with dynamically rotatable heterostructures. Science. 2018;361(6403):690–3.
[82] Hu C, Wu T, Huang X, Dong Y, Chen J, Zhang Z, et al. In-situ twistable bilayer graphene. Sci Rep. 2022;12(1):204.
[83] Kapfer M, Jessen BS, Eisele ME, Fu M, Danielsen DR, Darlington TP, et al. Programming twist angle and strain profiles in 2D materials. Science. 2023;381(6658):677–81.
[84] Cherepanov VV, Naumovets AG, Posudievsky OY, Koshechko VG, Pokhodenko VD. Self-assembly of the deposited graphene-like nanoparticles and possible nanotrack artefacts in AFM studies. Nano Express. 2020;1(1):010004.
[85] Gigli L, Manini N, Tosatti E, Guerra R, Vanossi A. Lifted graphene nanoribbons on gold: from smooth sliding to multiple stick-slip regimes. Nanoscale. 2018;10(4):2073–80.
[86] Finney NR, Yankowitz M, Muraleetharan L, Watanabe K, Taniguchi T, Dean CR, et al. Tunable crystal symmetry in graphene–boron nitride heterostructures with coexisting moiré superlattices. Nat Nanotechnol. 2019;14(11):1029–34.
[87] Li B, Yin J, Liu X, Wu H, Li J, Li X, et al. Probing van der Waals interactions at two-dimensional heterointerfaces. Nat Nanotechnol. 2019;14(6):567–72.
[88] Sarabadani J, Naji A, Asgari R, Podgornik R. Erratum: Many-body effects in the van der Waals–Casimir interaction between graphene layers. Phys Rev B. 2013;87(23):239905.
[89] Lifshitz EM, Hamermesh M. 26 - The theory of molecular attractive forces between solids, Reprinted from Soviet Physics JETP 2, Part 1, 73, 1956. In: Pitaevski LP, editor. Perspectives in theoretical physics. Amsterdam: Pergamon; 1992. p. 329–49.
[90] Kawai S, Benassi A, Gnecco E, Söde H, Pawlak R, Feng X, et al. Superlubricity of graphene nanoribbons on gold surfaces. Science. 2016;351(6276):957–61.
[91] Floría LM, Mazo JJ. Dissipative dynamics of the Frenkel-Kontorova model. Adv Phys. 1996;45(6):505–98.
[92] Eliaz N, Eliyahu M. Electrochemical processes of nucleation and growth of hydroxyapatite on titanium supported by real-time electrochemical atomic force microscopy. J Biomed Mater Res. 2007;80A(3):621–34.
[93] Macpherson JV, Unwin PR. Combined scanning electrochemical −atomic force microscopy. Anal Chem. 2000;72(2):276–85.
[94] Riss A, Paz AP, Wickenburg S, Tsai H-Z, De Oteyza DG, Bradley AJ, et al. Imaging single-molecule reaction intermediates stabilized by surface dissipation and entropy. Nat Chem. 2016;8(7):678–83.
[95] Zhang J, Chen P, Yuan B, Ji W, Cheng Z, Qiu X. Real-space identification of intermolecular bonding with atomic force microscopy. Science. 2013;342(6158):611–4.
[96] Li L, Wang M, Zhou Y, Zhang Y, Zhang F, Wu Y, et al. Manipulating the insulator–metal transition through tip-induced hydrogenation. Nat Mater. 2022;21(11):1246–51.

[97] Guardingo M, González-Monje P, Novio F, Bellido E, Busqué F, Molnár G, et al. Synthesis of nanoscale coordination polymers in femtoliter reactors on surfaces. ACS Nano. 2016;10(3):3206–13.
[98] Sung S, Park S, Lee W-J, Son J, Kim C-H, Kim Y, et al. Low-voltage flexible organic electronics based on high-performance sol-gel titanium dioxide dielectric. ACS Appl Mater Interfaces. 2015;7(14):7456–61.
[99] Gao Q, Tsai W-Y, Balke N. In situ and operando force-based atomic force microscopy for probing local functionality in energy storage materials. Electrochem Sci Adv. 2022;2(1):e2100038.
[100] Wang L, Wang D, Dong Z, Zhang F, Jin J. Interface chemistry engineering for stable cycling of reduced GO/SnO_2 nanocomposites for lithium ion battery. Nano Lett. 2013;13(4):1711–6.
[101] Cui C-H, Yu S-H. Engineering interface and surface of noble metal nanoparticle nanotubes toward enhanced catalytic activity for fuel cell applications. Acc Chem Res. 2013;46(7):1427–37.
[102] Wu G, Li P, Feng H, Zhang X, Chu PK. Engineering and functionalization of biomaterials via surface modification. J Mater Chem B. 2015;3(10):2024–42.
[103] Gosvami NN, Bares JA, Mangolini F, Konicek AR, Yablon DG, Carpick RW. Mechanisms of antiwear tribofilm growth revealed in situ by single-asperity sliding contacts. Science. 2015;348(6230):102–6.
[104] Avouris P, Hertel T, Martel R. Atomic force microscope tip-induced local oxidation of silicon: kinetics, mechanism, and nanofabrication. Appl Phys Lett. 1997;71(2):285–7.
[105] Masubuchi S, Arai M, Machida T. Atomic force microscopy based tunable local anodic oxidation of graphene. Nano Lett. 2011;11(11):4542–6.
[106] Zholdassov YS, Kwok RW, Shlain MA, Patel M, Marianski M, Braunschweig AB. Kinetics of primary mechanochemical covalent-bond-forming reactions. RSC Mechanochemistry. 2024;1(1):11–32.
[107] Tang C, Jiang Y, Chen C, Xiao C, Sun J, Qian L, et al. Graphene failure under MPa: Nanowear of step edges initiated by interfacial mechanochemical reactions. Nano Lett. 2024;24(13):3866–73.
[108] Kwon S, Ko J-H, Jeon K-J, Kim Y-H, Park JY. Enhanced nanoscale friction on fluorinated graphene. Nano Lett. 2012;12(12):6043–8.
[109] Ko J-H, Kwon S, Byun I-S, Choi JS, Park BH, Kim Y-H, et al. Nanotribological properties of fluorinated, hydrogenated, and oxidized graphenes. Tribol Lett. 2013;50(2):137–44.
[110] Li Q, Liu X-Z, Kim S-P, Shenoy VB, Sheehan PE, Robinson JT, et al. Fluorination of graphene enhances friction due to increased corrugation. Nano Lett. 2014;14(9):5212–7.
[111] Beyer MK, Clausen-Schaumann H. Mechanochemistry: the mechanical activation of covalent bonds. Chem Rev. 2005;105(8):2921–48.
[112] Kim MC, Hwang GS, Ruoff RS. Epoxide reduction with hydrazine on graphene: A first principles study. J Chem Phys. 2009;131(6):064704.
[113] Leenaerts O, Peelaers H, Hernández-Nieves AD, Partoens B, Peeters FM. First-principles investigation of graphene fluoride and graphane. Phys Rev B. 2010;82(19):195436.
[114] Kim H, Kim D-H, Jeong Y, Lee D-S, Son J, An S. Chemical gradients on graphene via direct mechanochemical cleavage of atoms from chemically functionalized graphene surfaces. Nanoscale Adv. 2023;5(8):2271–9.
[115] Raghuraman S, Elinski MB, Batteas JD, Felts JR. Driving surface chemistry at the nanometer scale using localized heat and stress. Nano Lett. 2017;17(4):2111–7.
[116] Raghuraman S, Soleymaniha M, Ye Z, Felts JR. The role of mechanical force on the kinetics and dynamics of electrochemical redox reactions on graphene. Nanoscale. 2018;10(37):17912–23.
[117] Ishii T, Kyotani T. Chapter 14 - Temperature programmed desorption. In: Inagaki M, Kang F, editors. Materials science and engineering of carbon. Oxford, United Kingdom: Butterworth-Heinemann; 2016. p. 287–305.
[118] Chen M. Chapter 12 - thermal analysis. In: Inagaki M, Kang F, editors. Materials science and engineering of carbon. Oxford, United Kingdom: Butterworth-Heinemann; 2016. p. 249–72.
[119] Wunderlich B. Thermal analysis. In: Buschow KHJ, Cahn RW, Flemings MC, Ilschner B, Kramer EJ, Mahajan S, et al., editors. Encyclopedia of materials: Science and technology. Oxford: Elsevier; 2001. p. 9134–41.
[120] Larciprete R, Fabris S, Sun T, Lacovig P, Baraldi A, Lizzit S. Dual path mechanism in the thermal reduction of graphene oxide. J Am Chem Soc. 2011;133(43):17315–21.
[121] Jung I, Field DA, Clark NJ, Zhu Y, Yang D, Piner RD, et al. Reduction kinetics of graphene oxide determined by electrical transport measurements and temperature programmed desorption. J Phys Chem C. 2009;113(43):18480–6.
[122] Jencks WP. A primer for the Bema Hapothle. An empirical approach to the characterization of changing transition-state structures. Chem Rev. 1985;85(6):511–27.
[123] Konda SSM, Brantley JN, Varghese BT, Wiggins KM, Bielawski CW, Makarov DE. Molecular catch bonds and the anti-hammond effect in polymer mechanochemistry. J Am Chem Soc. 2013;135(34):12722–9.
[124] Zhurkov SN. Kinetic concept of the strength of solids. Int J Fract. 1984;26(4):295–307.
[125] Coats AW, Redfern JP. Kinetic parameters from thermogravimetric data. Nature. 1964;201(4914):68–9.
[126] Bell GI. Models for the specific adhesion of cells to cells: A theoretical framework for adhesion mediated by reversible bonds between cell surface molecules. Science. 1978;200(4342):618–27.
[127] Roldán R, Castellanos-Gomez A, Cappelluti E, Guinea F. Strain engineering in semiconducting two-dimensional crystals. J Phys: Condens Matter. 2015;27(31):313201.
[128] Yu X, Peng Z, Xu L, Shi W, Li Z, Meng X, et al. Manipulating 2D materials through strain engineering. Small. 2024;20:2402561.
[129] Dai Z, Liu L, Zhang Z. Strain engineering of 2D materials: Issues and opportunities at the interface. Adv Mater. 2019;31(45):1805417.
[130] Ghorbani-Asl M, Borini S, Kuc A, Heine T. Strain-dependent modulation of conductivity in single-layer transition-metal dichalcogenides. Phys Rev B. 2013;87(23):235434.
[131] Feng J, Qian X, Huang C-W, Li J. Strain-engineered artificial atom as a broad-spectrum solar energy funnel. Nat Photonics. 2012;6(12):866–72.
[132] Tang D-M, Kvashnin DG, Najmaei S, Bando Y, Kimoto K, Koskinen P, et al. Nanomechanical cleavage of molybdenum disulphide atomic layers. Nat Commun. 2014;5(1):3631.
[133] Mohiuddin TMG, Lombardo A, Nair RR, Bonetti A, Savini G, Jalil R, et al. Uniaxial strain in graphene by Raman spectroscopy: G peak splitting, Gruneisen parameters, and sample orientation. Phys Rev B. 2009;79(20):205433.
[134] Wang Y, Cong C, Yang W, Shang J, Peimyoo N, Chen Y, et al. Strain-induced direct–indirect bandgap transition and phonon modulation in monolayer WS_2. Nano Res. 2015;8(8):2562–72.

[135] Hui YY, Liu X, Jie W, Chan NY, Hao J, Hsu Y-T, et al. Exceptional tunability of band energy in a compressively strained trilayer MoS_2 sheet. ACS Nano. 2013;7(8):7126–31.
[136] Plechinger G, Castellanos-Gomez A, Buscema M, van der Zant HSJ, Steele GA, Kuc A, et al. Control of biaxial strain in single-layer molybdenite using local thermal expansion of the substrate. 2D Mater. 2015;2(1):015006.
[137] Castellanos-Gomez A, Roldán R, Cappelluti E, Buscema M, Guinea F, van der Zant HSJ, et al. Local strain engineering in atomically thin MoS_2. Nano Lett. 2013;13(11):5361–6.
[138] Lu H, Bark C-W, Esque de los Ojos D, Alcala J, Eom CB, Catalan G, et al. Mechanical writing of ferroelectric polarization. Science. 2012;336(6077):59–61.
[139] Chaudhary P, Lu H, Loes M, Lipatov A, Sinitskii A, Gruverman A. Mechanical Stress Modulation of Resistance in MoS_2 Junctions. Nano Lett. 2022;22(3):1047–52.
[140] Fischer-Cripps AC. Introduction to contact mechanics. In: Frederick FL, editor. Mechanical engineering series. 2nd edn. New York: Springer; 2007.
[141] Deng Q, Lv S, Li Z, Tan K, Liang X, Shen S. The impact of flexoelectricity on materials, devices, and physics. J Appl Phys. 2020;128(8):080902.
[142] Wang B, Gu Y, Zhang S, Chen L-Q. Flexoelectricity in solids: Progress, challenges, and perspectives. Prog Mater Sci. 2019;106:100570.
[143] Yang R, Xu R, Dou W, Benner M, Zhang Q, Liu J. Semiconductor-based dynamic heterojunctions as an emerging strategy for high direct-current mechanical energy harvesting. Nano Energy. 2021;83:105849.
[144] Kogan SM. Piezoelectric effect during inhomogeneous deformation and acoustic scattering of carriers in crystals. Sov Phys-Solid State. 1964;5(10):2069–70.
[145] Tagantsev A. Piezoelectricity and flexoelectricity in crystalline dielectrics. Phys Rev B. 1986;34(8):5883.
[146] Yang M-M, Kim DJ, Alexe M. Flexo-photovoltaic effect. Science. 2018;360(6391):904–7.
[147] Feng P, Zhao S, Dang C, He S, Li M, Zhao L, et al. Improving the photoresponse performance of monolayer MoS_2 photodetector via local flexoelectric effect. Nanotechnology. 2022;33(25):255204.
[148] Pu D, Anwar MA, Zhou J, Mao R, Pan X, Chai J, et al. Enhanced photovoltaic effect in graphene–silicon Schottky junction under mechanical manipulation. Appl Phys Lett. 2023;122(4):041102.
[149] Wu H, Liu X, Yin J, Zhou J, Guo W. Tunable electrical performance of few-layered black phosphorus by strain. Small. 2016;12(38):5276–80.
[150] Gong C, Floresca HC, Hinojos D, McDonnell S, Qin X, Hao Y, et al. Rapid selective etching of PMMA residues from transferred graphene by carbon dioxide. J Phys Chem C. 2013;117(44):23000–8.
[151] Zhang J, Jia K, Lin L, Zhao W, Quang HT, Sun L, et al. Large-area synthesis of superclean graphene via selective etching of amorphous carbon with carbon dioxide. Angew Chem Int Ed. 2019;58(41):14446–51.
[152] Sun J, Finklea HO, Liu Y. Characterization and electrolytic cleaning of poly(methyl methacrylate) residues on transferred chemical vapor deposited graphene. Nanotechnology. 2017;28(12):125703.
[153] Wang X, Dolocan A, Chou H, Tao L, Dick A, Akinwande D, et al. Direct observation of poly(methyl methacrylate) removal from a graphene surface. Chem Mater. 2017;29(5):2033–9.
[154] Karlsson LH, Birch J, Mockute A, Ingason AS, Ta HQ, Rummeli MH, et al. Graphene on graphene formation from PMMA residues during annealing. Vacuum. 2017;137:191–4.
[155] Palumbo F, Lo Porto C, Favia P. Plasma nano-texturing of polymers for wettability control: Why, what and how. Coatings. 2019;9(10):640.
[156] Miyashita K, Tsunoura T, Yoshida K, Yano T, Kishi Y. Fluorine and oxygen plasma exposure behavior of yttrium oxyfluoride ceramics. Jpn J Appl Phys. 2019;58(SE):SEEC01.
[157] Min J-H, Lee J, Ayman MT, Kim H-N, Park Y-J, Yoon D-H. Plasma etching properties of various transparent ceramics. Ceram Int. 2020;46(3):2895–900.
[158] Ferrah D, Renault O, Marinov D, Arias-Zapata J, Chevalier N, Mariolle D, et al. CF4/H2 Plasma cleaning of graphene regenerates electronic properties of the pristine material. ACS Appl Nano Mater. 2019;2(3):1356–66.
[159] Mehedi HA, Ferrah D, Dubois J, Petit-Etienne C, Okuno H, Bouchiat V, et al. High density H2 and He plasmas: Can they be used to treat graphene? J Appl Phys. 2018;124(12):125304.
[160] Son BH, Kim HS, Jeong H, Park JY, Lee S, Ahn YH. Electron beam induced removal of PMMA layer used for graphene transfer. Sci Rep. 2017;7(1):18058.
[161] Materna Mikmeková E, Müllerová I, Frank L, Paták A, Polčák J, Sluyterman S, et al. Low-energy electron microscopy of graphene outside UHV: electron-induced removal of PMMA residues used for graphene transfer. J Electron Spectrosc Relat Phenom. 2020;241:146873.
[162] Tyler BJ, Brennan B, Stec H, Patel T, Hao L, Gilmore IS, et al. Removal of organic contamination from graphene with a controllable mass-selected argon gas cluster ion beam. J Phys Chem C. 2015;119(31):17836–41.
[163] Kim KS, Hong H-K, Jung H, Oh I-K, Lee Z, Kim H, et al. Surface treatment process applicable to next generation graphene-based electronics. Carbon. 2016;104:119–24.
[164] Hou Y, Dai Z, Zhang S, Feng S, Wang G, Liu L, et al. Elastocapillary cleaning of twisted bilayer graphene interfaces. Nat Commun. 2021;12(1):5069.
[165] Dong W, Dai Z, Liu L, Zhang Z. Toward clean 2D materials and devices: Recent progress in transfer and cleaning methods. Adv Mater. 2024;36(22):2303014.
[166] Ma C, Chen Y, Chu J. Time-dependent pinning of nanoblisters confined by two-dimensional sheets. Part 2: Contact line pinning. Langmuir. 2023;39(2):709–16.
[167] Jalilian R, Jauregui LA, Lopez G, Tian J, Roecker C, Yazdanpanah MM, et al. Scanning gate microscopy on graphene: charge inhomogeneity and extrinsic doping. Nanotechnology. 2011;22(29):295705.
[168] Lindvall N, Kalabukhov A, Yurgens A. Cleaning graphene using atomic force microscope. J Appl Phys. 2012;111(6):064904.
[169] Fessler G, Eren B, Gysin U, Glatzel T, Meyer E. Friction force microscopy studies on SiO2 supported pristine and hydrogenated graphene. Appl Phys Lett. 2014;104(4):041910.
[170] Choi W, Shehzad MA, Park S, Seo Y. Influence of removing PMMA residues on surface of CVD graphene using a contact-mode atomic force microscope. RSC Adv. 2017;7(12):6943–9.
[171] Deng S, Berry V. Wrinkled, rippled and crumpled graphene: an overview of formation mechanism, electronic properties, and applications. Mater Today. 2016;19(4):197–212.
[172] Rosenberger MR, Chuang H-J, McCreary KM, Hanbicki AT, Sivaram SV, Jonker BT. Nano-“Squeegee” for the creation of clean

2d material interfaces. ACS Appl Mater Interfaces. 2018;10(12):10379–87.
[173] Palai SK, Dyksik M, Sokolowski N, Ciorga M, Sánchez Viso E, Xie Y, et al. Approaching the intrinsic properties of moiré structures using atomic force microscopy ironing. Nano Lett. 2023;23(11):4749–55.
[174] Ding X, Qiao B, Chen H, Uzoma PC, Xu Y, Hu H, eds. Damage-free cleaning of 2D van der Waals heterostructures with nano-spherical AFM probes. 2023 IEEE 23rd International Conference on Nanotechnology (NANO). IEEE; 2023.
[175] Ding X, Qiao B, Uzoma PC, Anwar MA, Chen Y, Zhang L, et al. Nano-spherical tip-based smoothing with minimal damage for 2D van der Waals heterostructures. Nanoscale. 2025;17(6):3095–104.
[176] Schwartz JJ, Chuang H-J, Rosenberger MR, Sivaram SV, McCreary KM, Jonker BT, et al. Chemical identification of interlayer contaminants within van der Waals heterostructures. ACS Appl Mater Interfaces. 2019;11(28):25578–85.
[177] Kim Y, Herlinger P, Taniguchi T, Watanabe K, Smet JH. Reliable postprocessing improvement of van der Waals heterostructures. ACS Nano. 2019;13(12):14182–90.
[178] Talha-Dean T, Tarn Y, Mukherjee S, John JW, Huang D, Verzhbitskiy IA, et al. Nanoironing van der Waals heterostructures toward electrically controlled quantum dots. ACS Appl Mater Interfaces. 2024;16(24):31738–46.
[179] Chen S, Son J, Huang S, Watanabe K, Taniguchi T, Bashir R, et al. Tip-based cleaning and smoothing improves performance in monolayer MOS_2 devices. ACS Omega. 2021;6(5):4013–21.
[180] Hu H, Shi B, Breslin CM, Gignac L, Peng Y. A sub-micron spherical atomic force microscopic tip for surface measurements. Langmuir. 2020;36(27):7861–7.
[181] Fu T, Uzoma PC, Ding X, Wu P, Penkov O, Hu H. A novel nano-spherical tip for improving precision in elastic modulus measurements of polymer materials via atomic force microscopy. Micromachines. 2024;15(9):1175.
[182] Kaushal P, Khanna G. The role of 2-dimensional materials for electronic devices. Mater Sci Semicond Process. 2022;143:106546.
[183] Xu X, Pan Y, Liu S, Han B, Gu P, Li S, et al. Seeded 2D epitaxy of large-area single-crystal films of the van der Waals semiconductor 2H $MoTe_2$. Science. 2021;372(6538):195–200.
[184] Zhang W, Gao H, Deng C, Lv T, Hu S, Wu H, et al. An ultrathin memristor based on a two-dimensional WS_2/MoS_2 heterojunction. Nanoscale. 2021;13(26):11497–504.
[185] Zha J, Luo M, Ye M, Ahmed T, Yu X, Lien D-H, et al. Infrared photodetectors based on 2d materials and nanophotonics. Adv Funct Mater. 2022;32(15):2111970.
[186] Anwar MA, Ali M, Pu D, Bodepudi SC, Lv JH, Shehzad K, et al. Graphene-silicon diode for 2-d heterostructure electrical failure protection. IEEE J Electron Devices Soc. 2022;10:970–5.
[187] Salahuddin S, Ni K, Datta S. The era of hyper-scaling in electronics. Nat Electron. 2018;1(8):442–50.
[188] Hao Y, Xiang S, Han G, Zhang J, Ma X, Zhu Z, et al. Recent progress of integrated circuits and optoelectronic chips. Sci China Inf Sci. 2021;64(10):201401.
[189] Li S, Ma Y, Ouedraogo NAN, Liu F, You C, Deng W, et al. p-/n-Type modulation of 2D transition metal dichalcogenides for electronic and optoelectronic devices. Nano Res. 2022;15(1):123–44.
[190] Chakraborty S, Kumar H. 7 - Molecular dynamics simulations of two-dimensional materials. In: Yang E-H, Datta D, Ding J, Hader G, editors. Synthesis, modeling, and characterization of 2D materials, and their heterostructures. Amsterdam, Netherlands: Elsevier; 2020. p. 125–48.
[191] Momeni K, Ji Y, Wang Y, Paul S, Neshani S, Yilmaz DE, et al. Multiscale computational understanding and growth of 2D materials: a review. npj Comput Mater. 2020;6(1):22.
[192] Mianehrow H, Berglund LA, Wohlert J. Interface effects from moisture in nanocomposites of 2D graphene oxide in cellulose nanofiber (CNF) matrix – A molecular dynamics study. J Mater Chem A. 2022;10(4):2122–32.
[193] Majid A, Kanwal H, Khan SU, Ahmad A. A DFT study of structural and thermal properties of 2D layers. Int J Quantum Chem. 2021;121(11):e26625.
[194] Ladha DG. A review on density functional theory–based study on two-dimensional materials used in batteries. Mater Today Chem. 2019;11:94–111.
[195] Er D, Ghatak K. 6 - Atomistic modeling by density functional theory of two-dimensional materials. In: Yang E-H, Datta D, Ding J, Hader G, editors. Synthesis, modeling, and characterization of 2D materials, and their heterostructures. Amsterdam, Netherlands: Elsevier; 2020. p. 113–23.
[196] Michałowski M. Simulation model for frictional contact of two elastic surfaces in micro/nanoscale and its validation. Nanotechnol Rev. 2018;7(5):355–63.
[197] Kwawu CR, Aniagyei A, Konadu D, Limbey K, Menkah E, Tia R, et al. A DFT study of the oxygen reduction reaction mechanism on be doped graphene. Chem Pap. 2022;76(7):4471–80.
[198] Wang L, Zeng Z, Gao W, Maxson T, Raciti D, Giroux M, et al. Tunable intrinsic strain in two-dimensional transition metal electrocatalysts. Science. 2019;363(6429):870–4.
[199] Jeong JH, Kang S, Kim N, Joshi R, Lee G-H. Recent trends in covalent functionalization of 2D materials. Phys Chem Chem Phys. 2022;24(18):10684–711.
[200] Wang Z-G, Shen H-Y, Yu R-L, Gao J-F, Zhang G-Q, Xu C, et al. Universal production of functionalized 2D nanomaterials via integrating glucose-assisted mechanochemical exfoliation and cosolvent-intensified sonication exfoliation. Nano Res. 2022;16(4):5033–41.